Supporting information to:

Peptide-induced fractal assembly of silver nanoparticles for visual detection of disease biomarkers.

Maurice Retout†, Yash Mantri‡, Zhicheng Jin†, Jiajing Zhou†, Grégoire Noël₴, Brian Donovan†, Wonjun Yim†, Jesse V. Jokerst†§†,*

†Department of NanoEngineering, ‡Department of Bioengineering, §Materials Science and Engineering Program and †Department of Radiology, University of California, San Diego, La Jolla, CA 92093, United States

₴Functional and Evolutionary Entomology – Gembloux Agro-Bio Tech, University of Liège, 5030 Gembloux, Belgium

KEYWORDS. Coalescence, Colorimetric sensing, Fractal structures, Peptides, Silver nanomaterials

*Corresponding author's email: jjokerst@ucsd.edu

Table of Contents

1. Materials

Bis(*p*-sulfonatophenyl)phenylphosphine dihydrate dipotassium salt (BSPP, 97%), gold(III) chloride trihydrate ($HAuCl_4 \cdot 3H_2O$, >99.9%), sodium citrate tribasic dihydrate (>99%), Trizma® base (>99.9%), Trizma® hydrochloride (>90%), trifluoroacetic acid (TFA, HPLC grade, >99%), 2,2′-(ethylenedioxy)diethanethiol (EDDET, 95%), piperidine (ReagentPlus®, 99%) and Neuraminidase (NA) from *Clostridium perfringens* were purchased from Sigma Aldrich (St. Louis, MO). Trypsin (Tp), thrombin (Tb), hemoglobin (Hgb), and bovine serum albumin (BSA) were also purchased from Sigma Aldrich. Polyethylene glycol 2,000 (PEG_{2000}) was from Alfa Aesar (Tewksbury, MA). Thioanisole (>99%), N,N-diisopropylethylamine (DIPEA, >99%), and triisopropylsilane (TIPS, >98%) were purchased from Tokyo Chemical Industry Co., Ltd. (TCI). Sodium chloride (certified ACS), sodium phosphate monobasic monohydrate (certified ACS), and sodium phosphate dibasic anhydrous (certified ACS) were purchased from Fisher Scientific International, Inc. (Hampton, NH).

Fmoc-protected L/D-amino acids, hexafluorophosphate benzotriazole tetramethyl uronium (HBTU), and Fmoc-Rink amide MBHA resin (0.67 mmol/g, 100-150 mesh) were purchased from AappTec, LLC (Louisville, KY). The main protease (Mpro) of SARS-CoV-2 was given as kind gifts from Dr. Anthony O'Donoghue, UC San Diego, USA. The Mpro was stored in 20 mM Tris-HCl (pH 8.0), with 150 mM NaCl, 1 mM DTT, and 5 % glycerol at −80 °C. The Painpin-like protease (PLpro) was given as kind gift from Dr. Shaun K. Olsen, UT Health San Antonio, USA. The PLpro was stored in 20 mM Tris-HCl (pH 8.0), with 150 mM NaCl, 1 mM DTT, and 5 % glycerol at −80 °C. The pooled whole human saliva was purchased from Lee Biosolutions, Inc. (Maryland Heights, MO). The exhaled breath condensation (EBC) was collected from healthy volunteers (COVID-negative) using a lab condensate tube set-up under IRB approval at UC San Diego.

Organic solvents including N,N-dimethylformamide (DMF, sequencing grade), acetonitrile (ACN, HPLC grade), ethyl ether (certified ACS), methylene chloride (DCM, certified ACS), and dimethyl sulfoxide (DMSO, certified ACS) were from Fisher Scientific International, Inc. (Hampton, NH). D_2O solvent for ^1H NMR experiments was purchased from Cambridge Isotope Laboratories (Andover, MA). Ultrapure water (18 MΩ·cm) was obtained from a Milli-Q Academic water purification system (Millipore Corp., Billerica, MA). TEM grids (formvar/carbon 300 mesh Cu) were purchased from Ted Pella (Redding, CA). Amicon® ultra-15 centrifugal filter units (M.W. cutoff =100 kDa) and automation compatible syringe filters (PTFE, 0.45 mm) were from MilliporeSigma (St. Louis, MO). Glassware and stir bars were cleaned with aqua regia ($HCl:HNO_3$=3:1 by volume) and boiling water before use. Peptides RRK, $(RRK)_2$, $(RRK)_3$, HHK, TSAVLQ (M4), and CKLVFF were purchased from Genscript Inc. (New Jersey, USA). Citrate-capped silver nanoparticles (AgNPs-citrate) were purchased from Nanocompsix (San Diego, USA).

2. Instrumentation

The optical absorption measurements were collected using a hybrid multi-mode microplate reader (Synergy™ H1 model, BioTek Instruments, Inc.) in a 96-well plate. Peptides TSG, TRG, TRK, RR, DDGDSFRHHK, FFK, SGFRRGRR, M1, M2, and M3 were synthesized using an automated Eclipse™ peptide synthesizer (AAPPTec, Louisville, KY) through standard solid phase Fmoc syntheses on Rink-amide resin (see below). Peptides TSG, TRG, TRK, RR, DDGDSFRHHK, FFK, SGFRRGRR, M1, M2, and M3 were lyophilized in a FreeZone Plus 2.5 freeze dry system (Labconco Corp., Kansas, MO). Peptides TSG, TRG, TRK, RR, DDGDSFRHHK, FFK, SGFRRGRR, M1, M2, and M3 purification was carried out using a Shimadzu LC-40 HPLC system equipped with a LC-40D solvent delivery module, photodiode array detector SPD-M40, and degassing unit DGU-403. The sample was dissolved in water and acetonitrile and applied on a Zorbax 300 BS, C18 column (5 mm, 9.4×250 mm) from Agilent, and eluted at 1.5 mL/min with a 40 min gradient from 10% to 95% solvent B. Here, solvent A is water (0.05% TFA) and solvent B is acetonitrile (0.05% TFA). Preparative injections were monitored at 190, 220, and 254 nm. All products were purified by HPLC to reach purity of >90%.

Electrospray ionization mass spectrometry (ESI-MS) data was acquired by using a Micromass Quattro Ultima mass spectrometer in the Molecular MS Facility (MMSF) at Chemistry and Biochemistry Department, UC San Diego. ESI-MS samples were prepared in a 50% MeOH/H_2O mixture. Peptide concentration was determined using a NanoDrop™ One UV-vis spectrophotometer (Thermo Fisher Scientific, Waltham, MA). The dynamic light scattering (DLS) and zeta (z) potential measurements were carried out using a compact Zetasizer Nano ZS90 (Malvern Panalytical, Inc.). Transmission electron microscopy (TEM) images of the Au colloids were acquired using a JEOL 1200 EX II operated at 80 kV. The TEM grids were prepared by drop casting samples in water (2 mL) followed by natural drying. The inductively coupled plasma mass spectrometry (ICP-MS) analysis was performed using a Thermo Scientific iCAP RQ ICP–MS in the Environmental and Complex Analysis Laboratory at UC San Diego.

The multispectral advanced nanoparticle tracking analysis (MANTA) were performed with the ViewSizer 3000 (Horiba scientific, CA, USA). The temperature was set up to 25 °C during the measurement. Automated noise analysis determines the optimal wavelength for representing each nanoparticle. Here, 8-bit composite videos were generated, and 10 videos were used per analysis (300 frames for seconds). A quartz cuvette with minimum volume of 0.8 mL was used for the measurement.

The inductively coupled plasma mass spectrometry (ICP-MS) analysis was performed using a Thermo Scientific iCAP RQ ICP-MS in the environmental and complex analysis laboratory at UCSD. Samples were digested and diluted in 10 ml of 4% of HNO_3. Laser powers were maintained constant through all experiments. Samples were characterized by XRD with the Bruker D8 Advance used in Bragg–Brentanno geometry. Cu radiation: 1.54 Angstroms, equipped with a Ni K-beta filter. The 2θ scan range was 10–80° in increments of 0.02 and exposure of 0.25 seconds per scan. Energy-dispersive X-ray spectroscopy (EDX) profiles were acquired using ThermoFisher Talos 200X instrument with an operating voltage of 200 kV.

3. AgNPs-BSPP synthesis

BSPP-coated silver nanoparticles (AgNPs-BSPP) were synthesized via a two steps procedure: First, 60 µL of an aqueous solution of sodium borohydride ($NaBH_4$) (0.1 M) was added to 6 mL of an aqueous solution of silver nitrate (0.1 mM) under vigorous stirring in a glass vial containing a magnetic stir bar. The color of the suspension instantaneously turned from clear to light yellow. After 10 minutes, the color of the solution became more pronounced yellow, thus indicating the formation of small silver nanospheres (seeds). The resulting solution was stirred for 16 hours (overnight) and then 400 µL of an aqueous solution of sodium ascorbate ($C_6H_7O_6.Na$) (15 mM) was added followed by 200 µL of an aqueous solution of BSPP (5 mM). The resulting solution was stirred for 10 minutes followed by step-wise addition of silver nitrate (1 mM). In detail, 10 additions of 400 µL of silver nitrate (1 mM) every 30 seconds with an addition time of approximately five seconds. The role of ascorbate is to maintain a reducing environment and prevent the dissolution of the AgNPs by the BSPP. The color of the suspension turned golden-yellow indicating the formation of larger particles. Finally, 400 µL of BSPP (5 mM) was added, and the resulting solution was stirred for 48 hours. The resulting AgNPs-BSPP were stored in the reaction medium at room temperature. Figure S1a shows a scheme of the procedure. The freshly synthesized particles express a maximum of light absorption at 400 nm (Figure S3) that gives to their suspension a bright yellow color (Figure S2b).

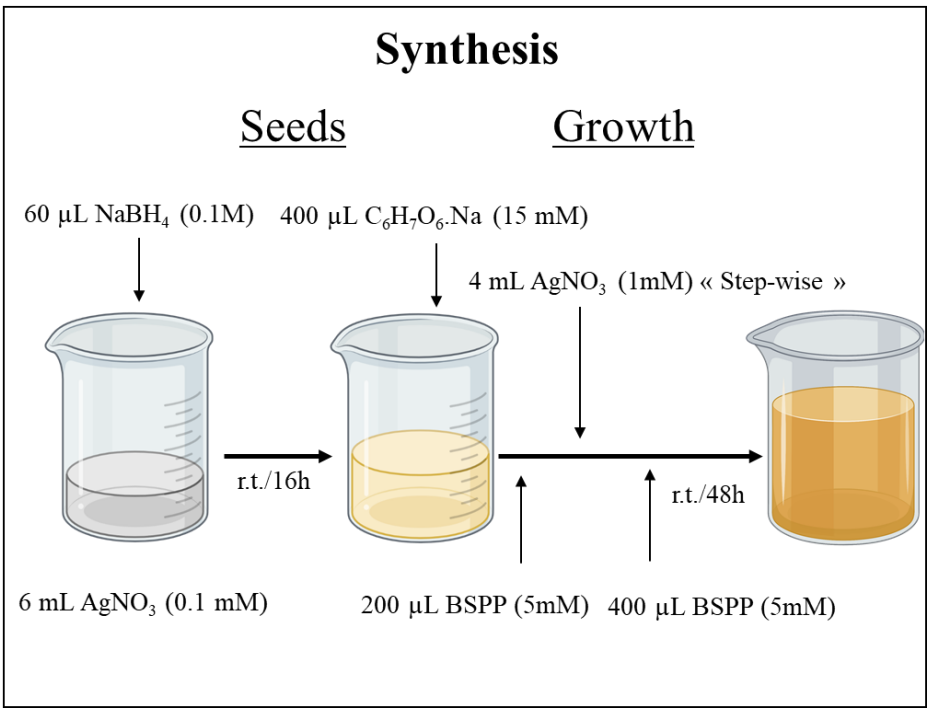

Figure S1 Illustration of the synthesis procedure.

The choice of a two steps synthesis was motivated by the impossibility to produce silver nanoparticles with a one-step procedure. Indeed, the BSPP interact strongly with silver ions, thus cancelling their reduction into particles (See Figure S2a). Similarly, increasing the concentration of BSPP after the formation of silver seeds decreases the number of particles formed as indicated by a less intense color (Figure S2b, S2c, S2d, S2e and S2f).

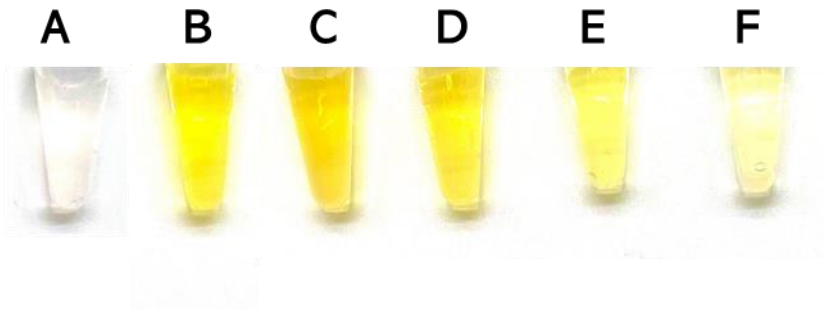

Figure S2 Picture of AgNPs-BSPP synthesized with (a) BSPP added before the $NabH_4$ addition or via the standard procedure with (b) 200 µL of BSPP, (c) 400 µL of BSPP, (d) 800 µL of BSPP, (e) 1600 µL of BSPP, or (f) 3200 µL of BSPP.

Scale-up of the synthesis has been investigated by increasing the initial concentration of $AgNO_3$ from 0.1 mM to 1 mM. Concentrations above 0.5 mM lead to highly aggregated AgNPs-BSPP, thus leading to a dull-grey color. Concentrations between 0.1 mM and 0.5 mM lead to AgNPs-BSPP with a broad size distribution. We concluded that increasing the concentrations was not a suitable approach to scaling-up the synthesis. Subsequently, we increased the reaction volume. This led to 1 L of AgNPs-BSPP with a size distribution identical to the ones produced in smaller scale. Figure S3 shows that the LSPR band of scale-up AgNPs-BSPP is similar to the small-scale AgNPs-BSPP.

The AgNPs-BSPP were characterized by UV-Vis spectroscopy, TEM, EDS, and XRD. The AgNPs-BSPP absorb strongly light around 400 nm with a bright yellow color (Figure S3). The AgNPs-BSPP have a spherical shape with a core diameter of approximately 20 nm (22.6 ± 4.3 nm) (Figure S4 and S5). EDX analysis of AgNPs-BSPP revealed the presence of mostly silver on the particles with few phosphorus, carbon, and sulfur coming for the BSPP. No sodium, mercury, or gold was observed (Figure S6).

XRD analysis revealed the face-centered crystal structure of the AgNPs-BSPP with peaks at 38.9°, 44.4°, 64.8°, and 78.1° corresponding to a Miller index of (1,1,1), (2,0,0), (2,2,0), and (3,1,1), respectively (Figure S7). Finally, the surface potential of the particles was measured to be -15 mV.

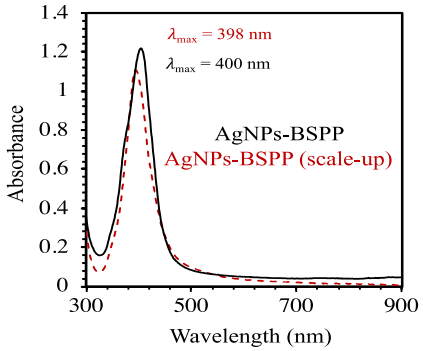

Figure S3 UV-Vis spectra of AgNPs-BSPP (black plain line) and AgNPs-BSPP synthesized via the scale-up procedure.

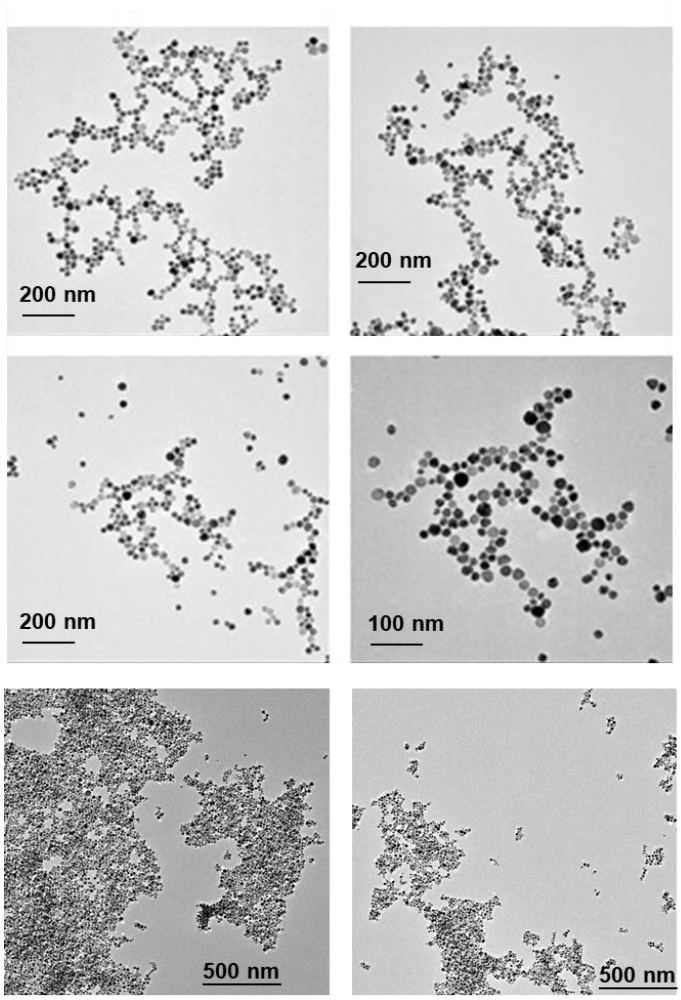

Figure S4 TEM images of the AgNPs-BSPP.

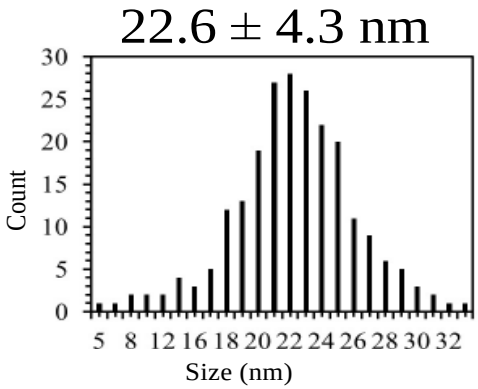

Figure S5 Histogram of the size distribution of the AgNPs-BSPP generated from the measurement of more than 200 AgNPs using Pebbles software.[1]

[1] S. Mondini, A. M. Ferretti, A. Puglisi, A. Ponti, *Nanoscale* **2012**, *4*, 5356–5372.

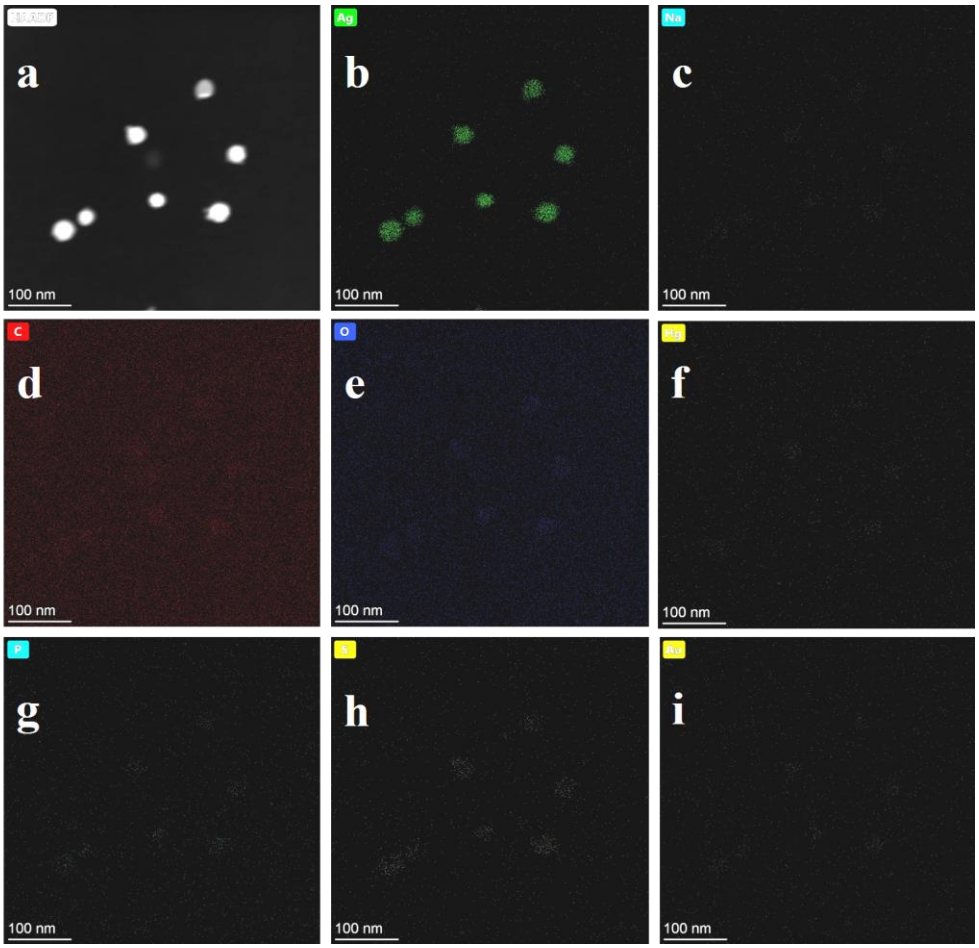

Figure S6 EDX analysis of AgNPs-BSPP with (a), (b) silver, (c) sodium, (d) carbon, (e) oxygen, (f) mercury, (g) phosphorus, (h) sulfur, and (i) gold.

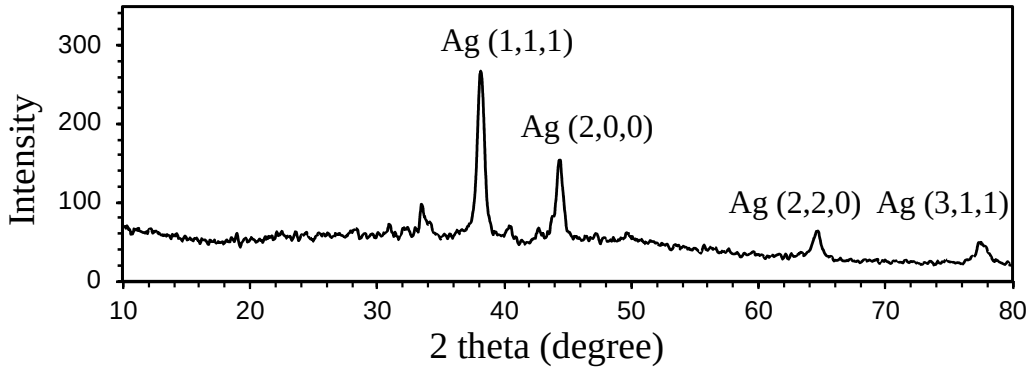

Figure S7 XRD spectrum of AgNPs-BSPP.

4. Peptide synthesis

Peptides TSG, TRG, TRK, RR, FFK, DDGDSFRHHK, SGFRRGRR, M1, M2, and M3 were made using standard Fmoc synthesis on an Aapptec eclipse personal peptide synthesizer. Wang resin was used as the solid support for all peptides and was cleaved using a mixture of TFA/EODT/thioanisole/anisole (88:5:5:2, v/v) for 3 h under an argon blanket. The freshly cleaved peptide was precipitated in −80 °C diethyl ether and washed several times (3×) using centrifugation. After the final centrifugation cycle, diethyl ether was decanted and the white peptide slurry was dissolved in an H_2O/glacial acetic acid mixture (90:10, v/v) to ensure TFA salt replacement with acetate salt during lyophilization. The peptide was frozen, lyophilized overnight, and then stored at −20 °C under an argon blanket.

Peptide purification was carried out using a Shimadzu LC-40 HPLC system equipped with a LC-40D solvent delivery module, photodiode array detector SPD-M40, and degassing unit DGU-403. The sample was dissolved in water and acetonitrile, applied on a Zorbax 300 BS, C18 column (5 mm, 9.4×250 mm) from Agilent, and eluted at 1.5 mL/min with a 40 min gradient from 10% to 95% of acetonitrile in water (with 0.05% TFA). Preparative injections were monitored at 190, 220, and 254 nm. All products were purified by HPLC to reach purity of >90%.

Peptide synthesis was confirmed using Electrospray ionization mass spectrometry (ESI-MS) via the Micromass Quattro Ultima mass spectrometer in the Molecular MS Facility (MMSF) at Chemistry and Biochemistry Department, UC San Diego. ESI-MS samples were prepared in a 50% MeOH/H_2O mixture. Peptide concentration was determined using a NanoDrop™ One UV-vis spectrophotometer (Thermo Fisher Scientific, Waltham, MA).

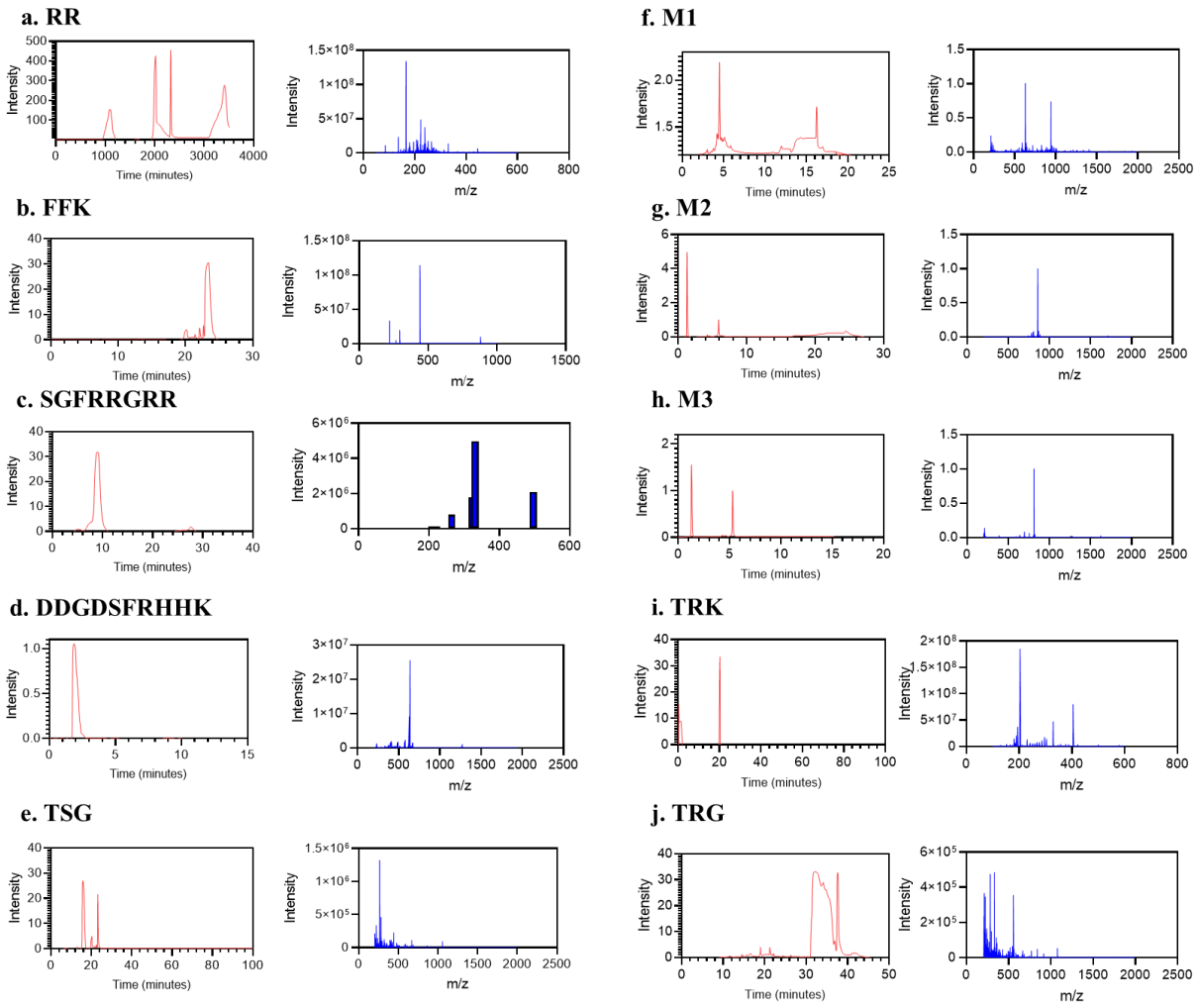

Figure S8. HPLC and ESI-MS data of the synthesized peptides. HPLC is shown in the left panel, and MS in the right panel. **(a-e)** Data collected from RR, FFK, SGFRRGRRK, DGDSFRHHK and TSG. **(f-h)** Data collected from M1, M2, M3, TRK and TRG.

5. Fractal assembly characterization

Peptide density calculation: An online peptide calculator from Northwestern University was used to determine a theoretical volume of 555 A^3 for the RRK peptide (URL : http://biotools.nubic.northwestern.edu/proteincalc.html). We then considered the peptide RRK to be a sphere and determined a surface aera of 0.8 nm^2 for one peptide. This corresponds to approximately 1.3 RRK per nm^2. Considering the surface of one AgNPs as 1250 nm^2, the addition of 1 µM of RRK to a 0.3 nM suspension of AgNPs corresponds to approximately 2.6 RRK/nm^2 that is twice the maximal density (1.3/nm^2) calculated previously.

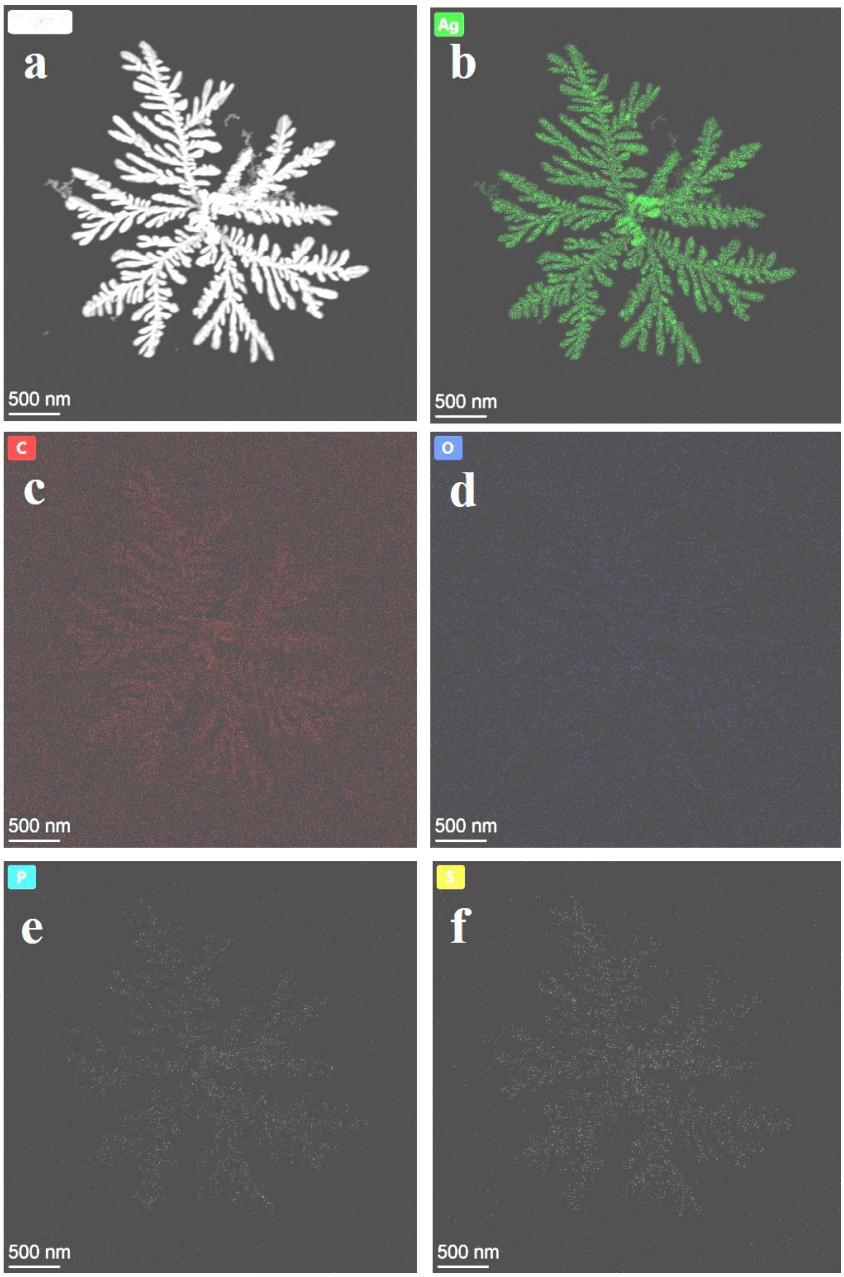

Figure S9 EDX analysis of AgNPs-BSPP in the presence of 1 µM of RRK showing the composition of (b) silver, (c) carbon, (d) oxygen, (e) phosphorus, and (f) sulfur.

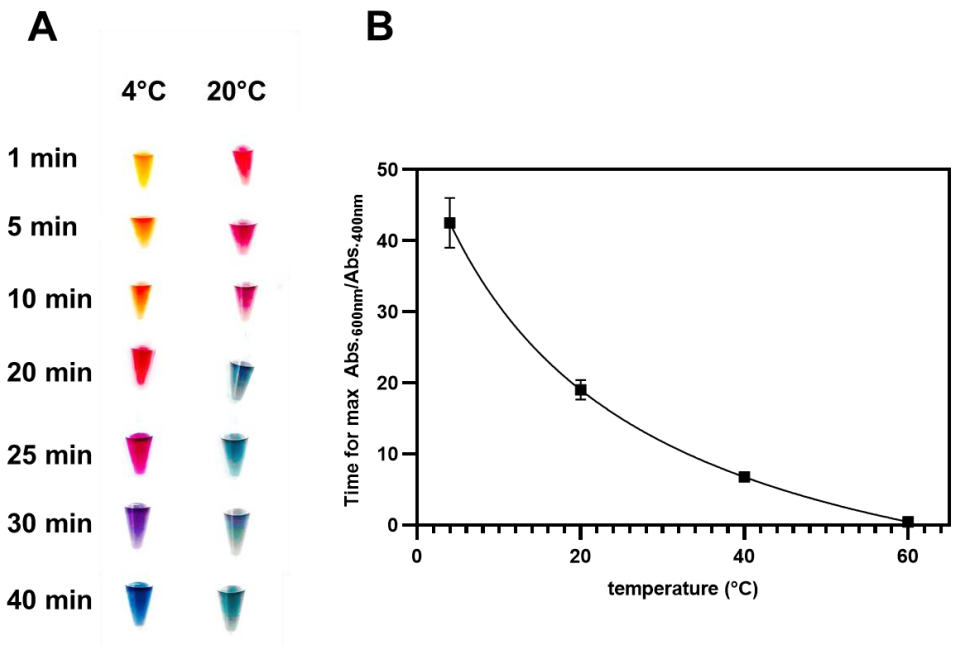

Figure S10 (A) Evolution of the change of color of AgNPs-BSPP mixed with 1 µM of RRK over time either at 4°C (left) or 20 °C (right). **(B)** Time in minutes for the AgNPs-BSPP mixed with 1 µM of RRK to reach the maximal ratio $Abs._{600\ nm}/Abs._{400\ nm}$ as a function of the temperature.

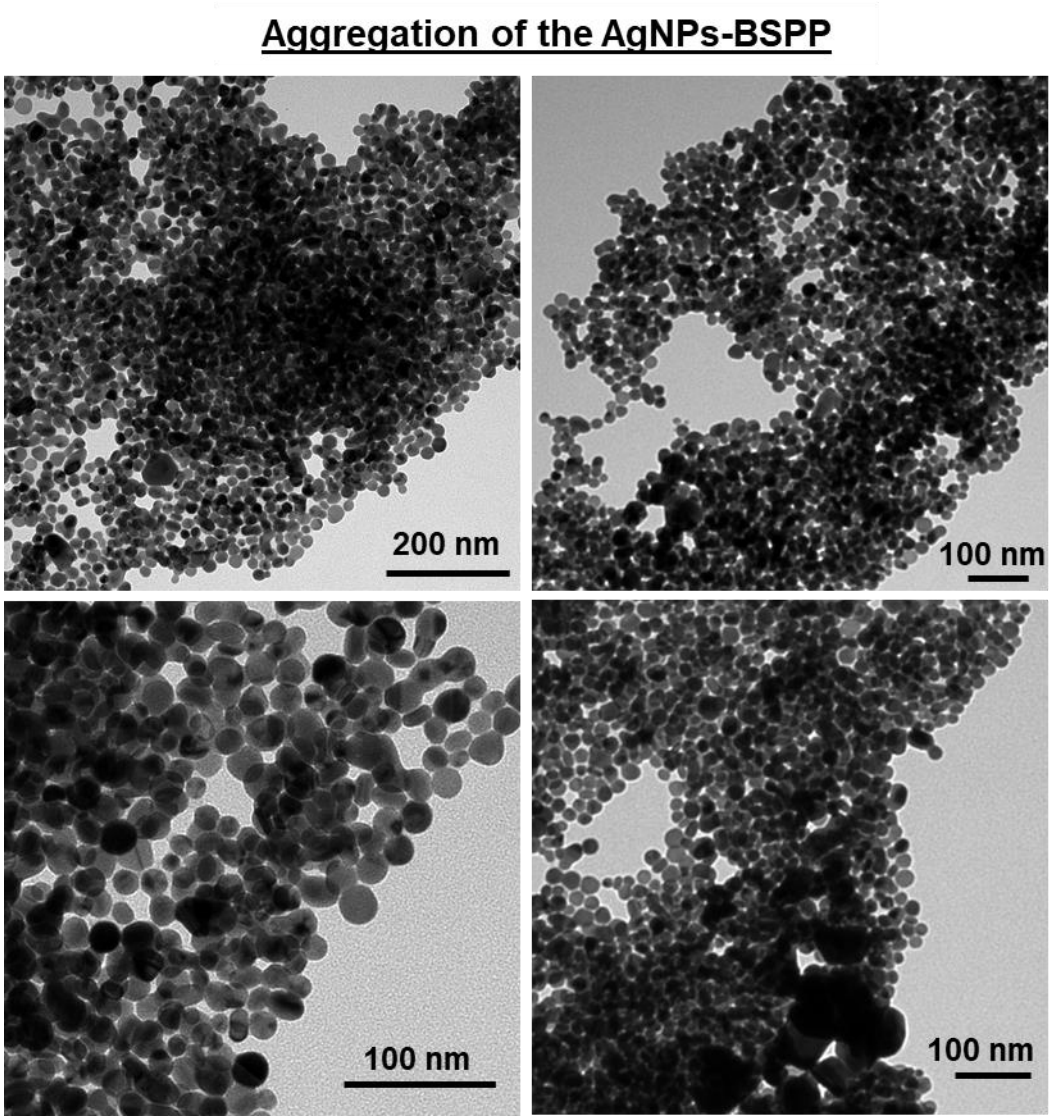

Figure S11 TEM pictures of AgNPs-BSPP taken between 1 and 3 minutes after the addition of 1 µM of RRK at 4°C.

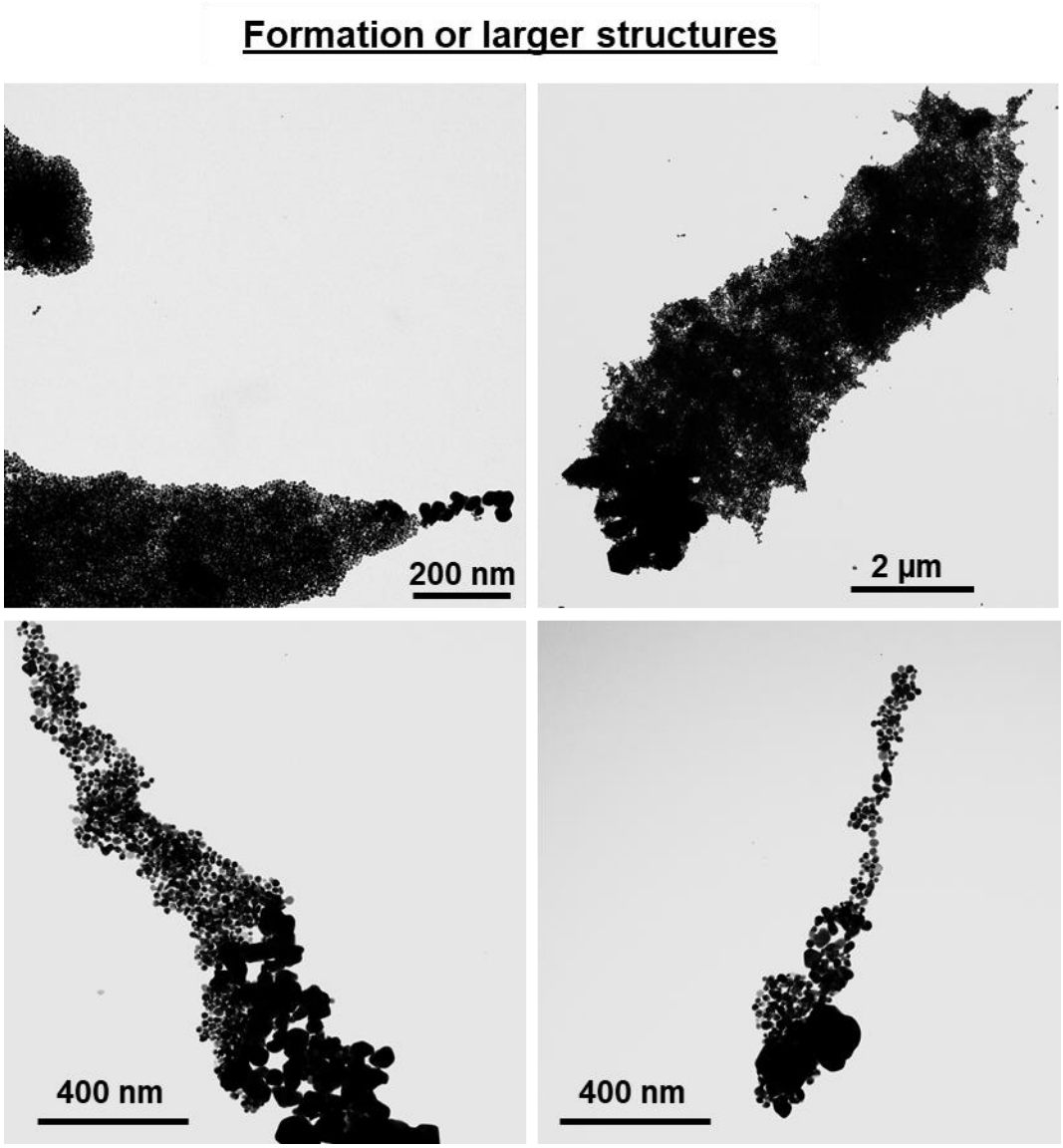

Figure S12 TEM pictures of AgNPs-BSPP taken between 6 and 9 minutes after the addition of 1 µM of RRK at 4°C.

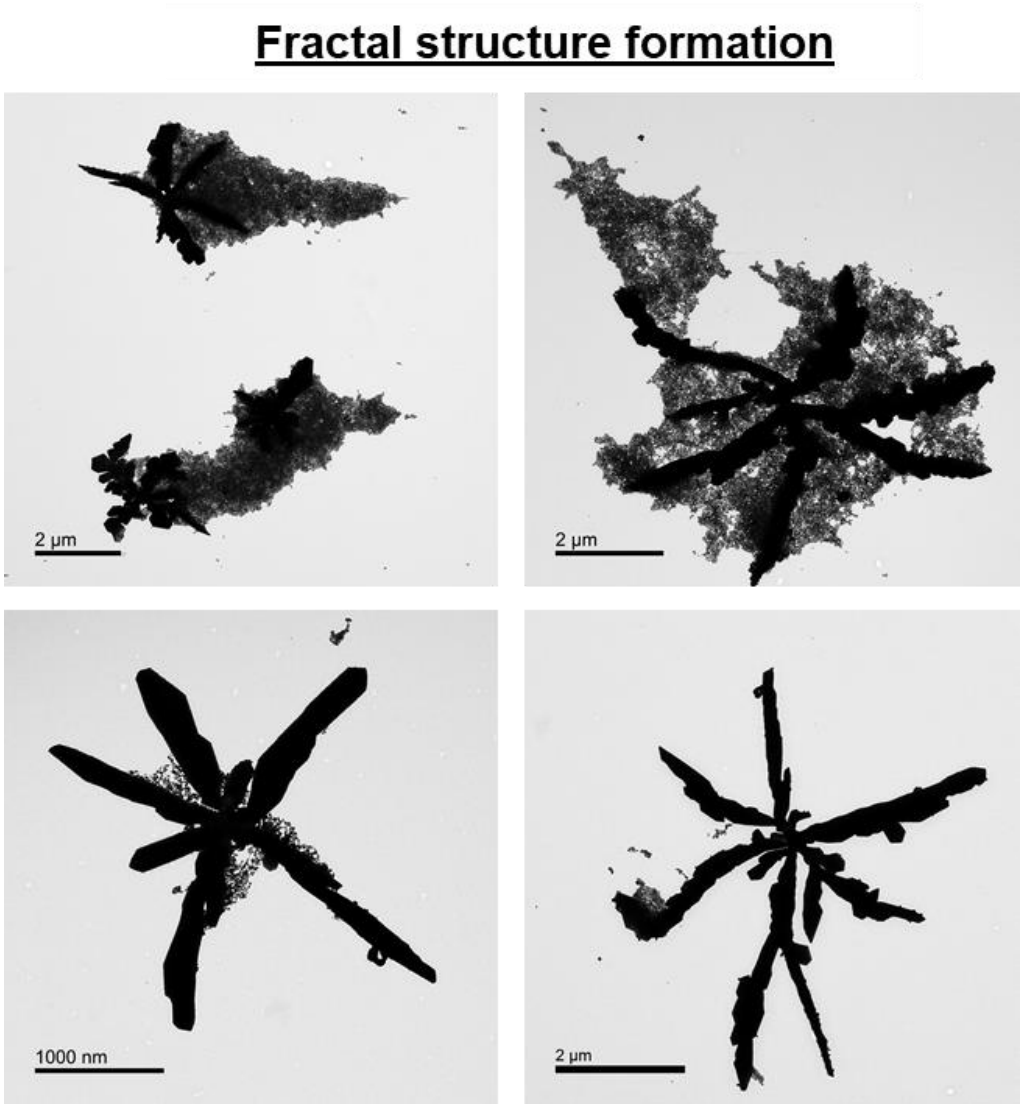

Figure S13 TEM pictures of AgNPs-BSPP taken between 12 and 15 minutes after the addition of 1 µM of RRK at 4°C.

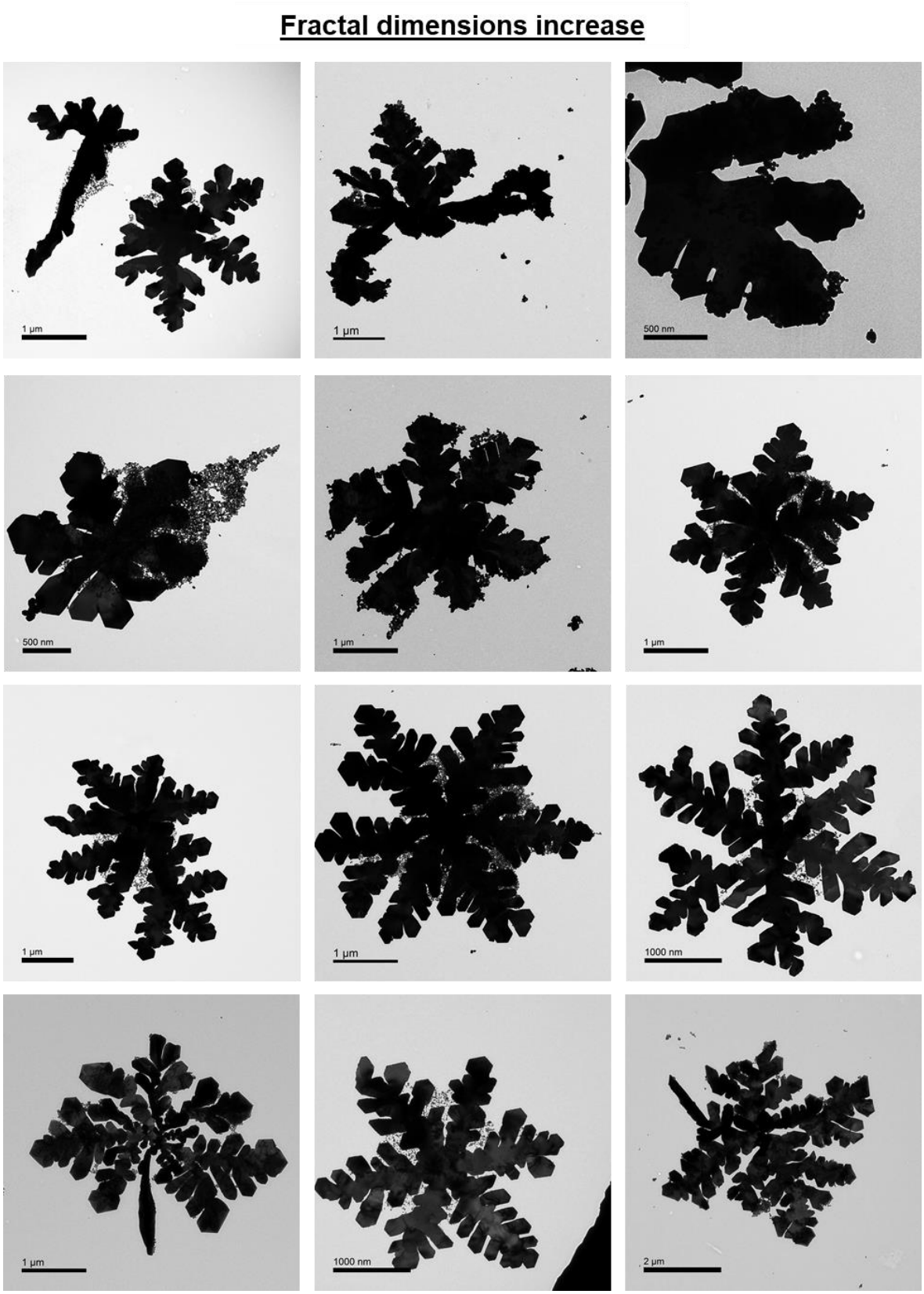

Figure S14 TEM pictures of AgNPs-BSPP taken between 18 and 30 minutes after the addition of 1 µM of RRK at 4°C.

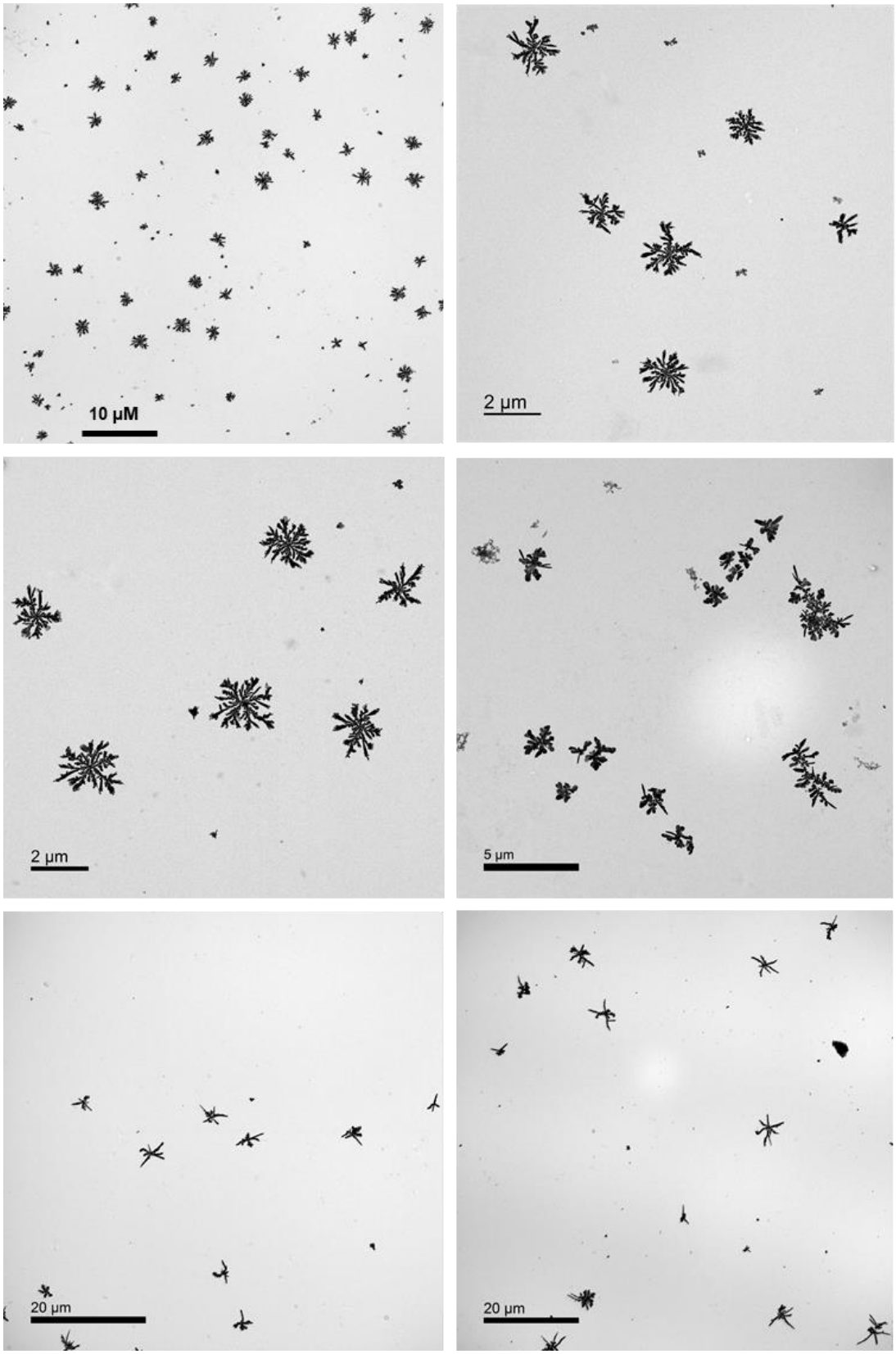

Figure S15 TEM pictures of AgNPs-BSPP after the addition of 1 µM of RRK at low magnification.

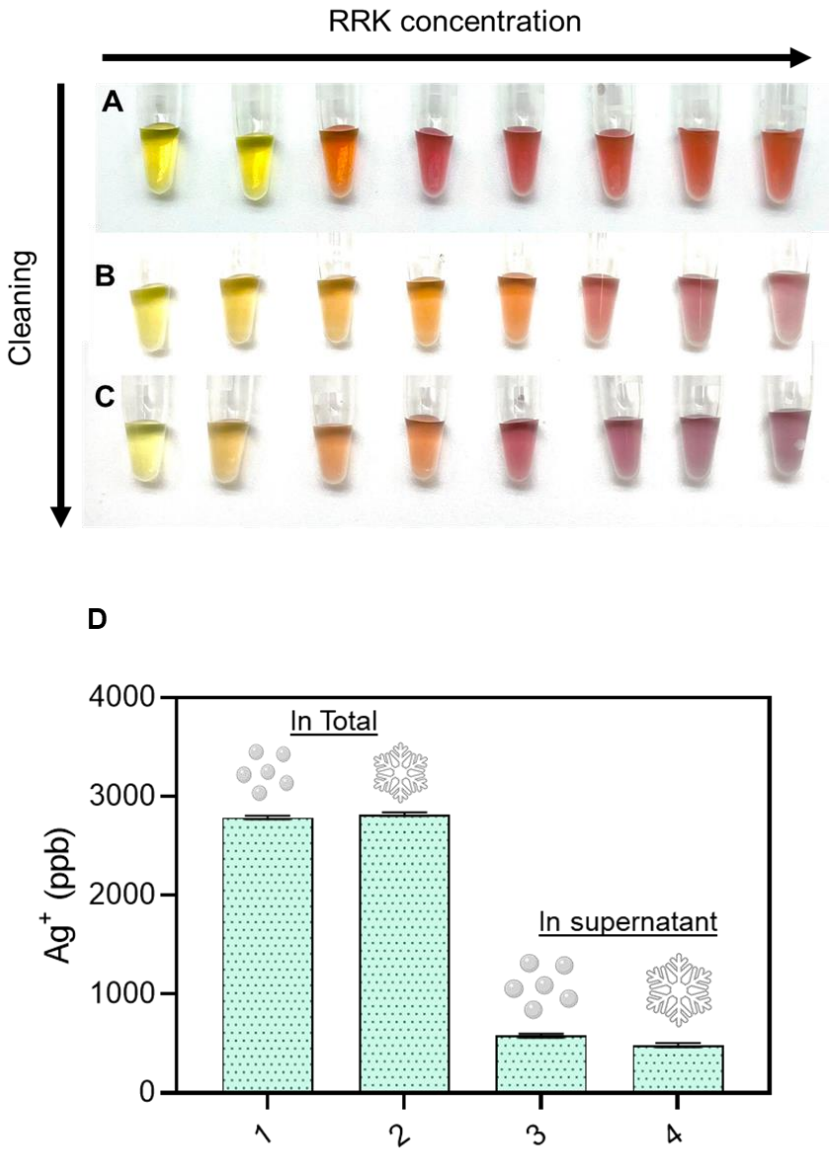

Figure S16 Pictures of several samples of AgNPs-BSPP 15 minutes after the addition of increasing concentrations of RRK in the case of **(A)** non-cleaned particles or **(B)** particles cleaned once, or **(C)** particles cleaned twice. Cleaning cycles consist of centrifugation, removal of the supernatant, and replacement with milliQ water. **(D)** ICP measurements of the total concentration or the concentration in the supernatant (free silver ions) of silver ions for AgNPs-BSPP (1 and 3) before or (2 and 4) after the reaction with 1 µM of RRK

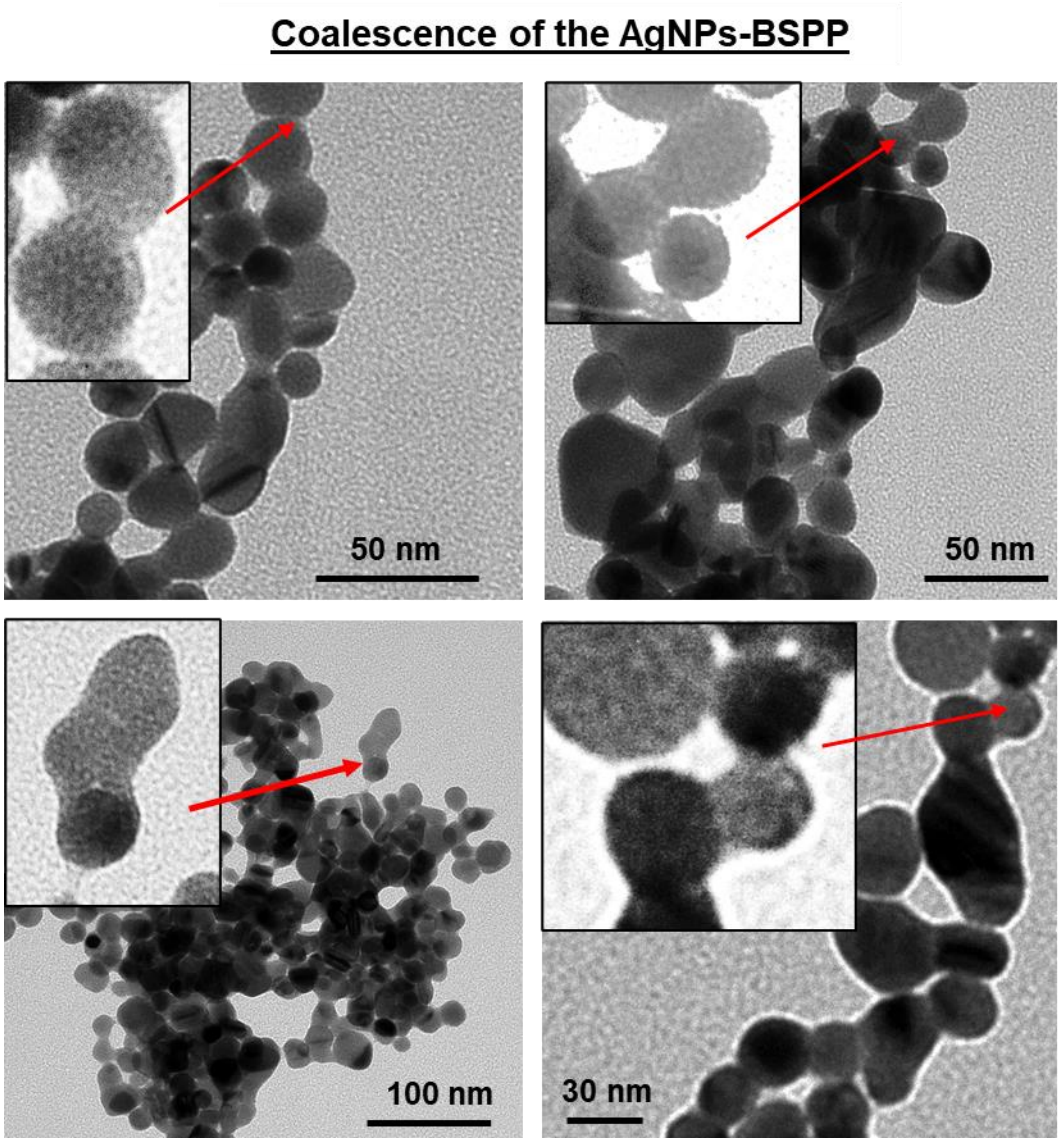

Figure S17 TEM pictures of AgNPs-BSPP taken between 1 and 3 minutes after the addition of 1 µM of RRK at 4°C.

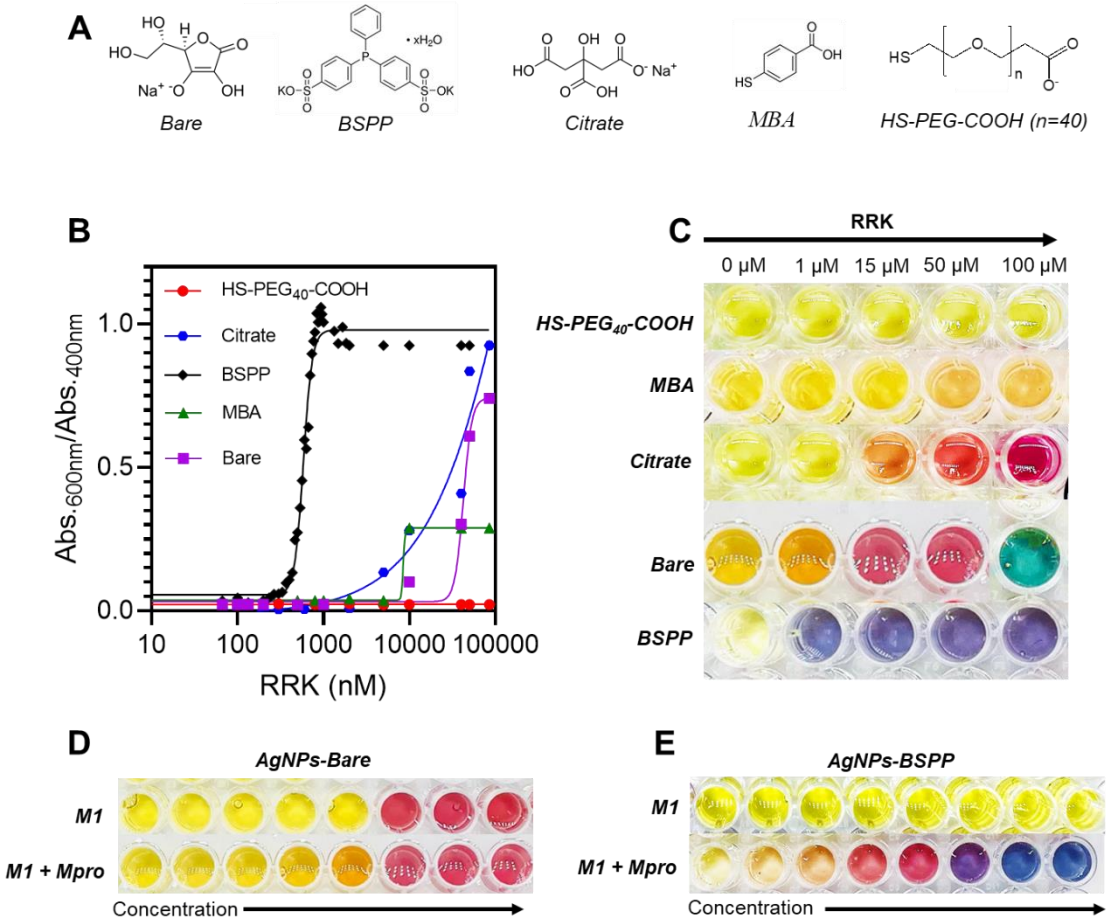

Figure S18 (A) Structures of the ligands investigated. **(B)** Ratio of the absorbance at 600 nm and 400 nm as a function of the concentration of RRK. **(C)** Samples of AgNPs-BSPP, -Bare, -citrate, -MBA or -S-PEG-COOH exposed to different concentration of RRK. **(D) and (E)** Images of the AgNPs-Bare (D) or AgNPs-BSPP (E) 15 minutes after the addition of increasing concentrations of either the peptide M1 or the peptide M1 cleaved by Mpro.

<u>AuNPs-BSPP synthesis:</u> First, citrate-stabilized AuNPs (~13 nm diameter, TEM) were prepared using Turkevich method by rapidly injecting an aqueous solution of sodium citrate tribasic dihydrate (150 mg, 5 mL) into an aqueous solution of $HAuCl_4 \cdot 3H_2O$ (45 mg, 300 mL) under boiling conditions and vigorous stirring. The reaction mixture was left boiling while stirring for another 15 min, and then cooled down to room temperature. The deep red dispersion was then purified by applying one round of centrifugation at 18,000 *g* for 30 min and the pink supernatant was discarded. The resulting pellet of citrate-AuNPs was redispersed in DI water by sonication and stored at ambient conditions.

The ligand exchange was carried out as below. A stock citrate-AuNP dispersion in water (200 mL, 3.4 nM) was vigorously stirred overnight with BSPP (205 mg, 5 mL) in a round bottom flask. The mixture was purified via syringe filtration (PTFE, 0.45 mm) followed by two rounds of centrifugation at 18,000 *g* for 40 min each. The resulting

pellet of BSPP-AuNPs was redispersed in DI water at an optical density of 1.5 (*c* ~3.8 nM, ε_{520}=4.0×10^{8} M^{-1}cm^{-1}) and stored at 4 °C for use.

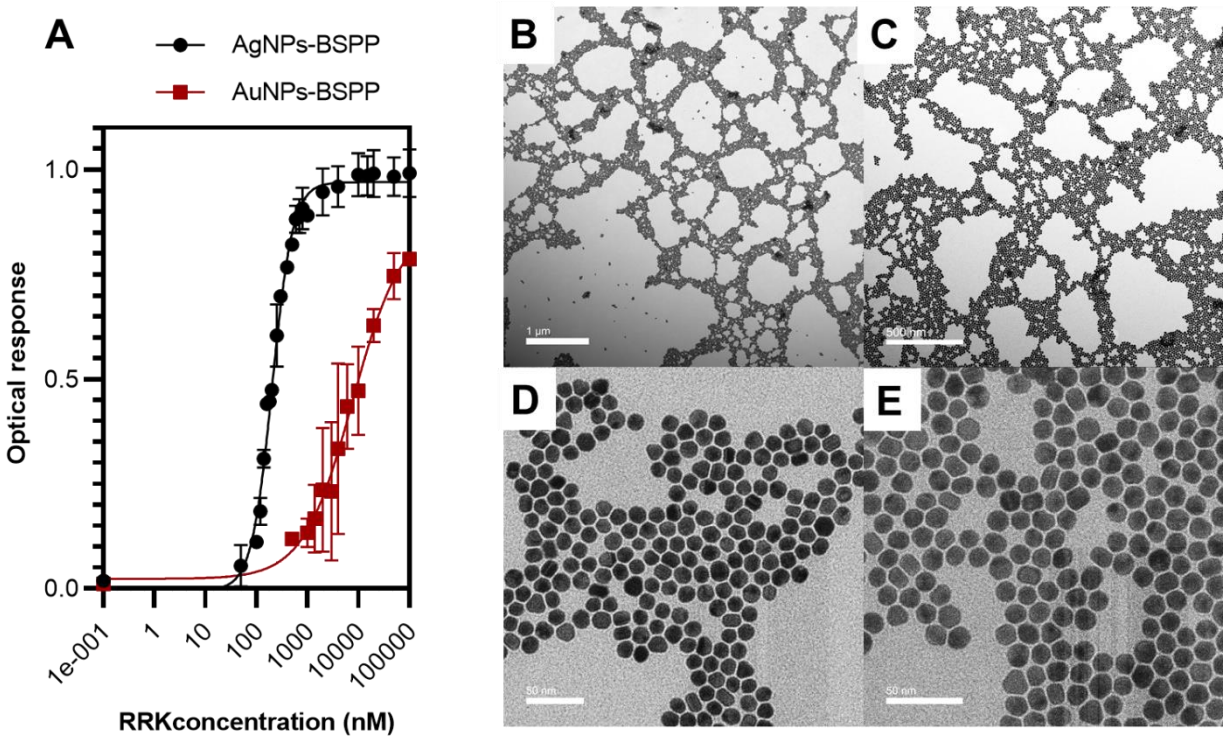

Figure S19 (A) Optical response of AuNPs-BSPP vs AgNPs-BSPP as a function of the concentration of RRK. Optical response = Abs.$_{600\ nm}$/Abs.$_{400\ nm}$ for AgNPs-BSPP and Abs.$_{620nm}$/Abs.$_{520nm}$ **(B), (C), (D)** and **(E)** TEM images of the AuNPs-BSPP exposed to 100 µM of RRK.

6. Control of the assembly with peptides

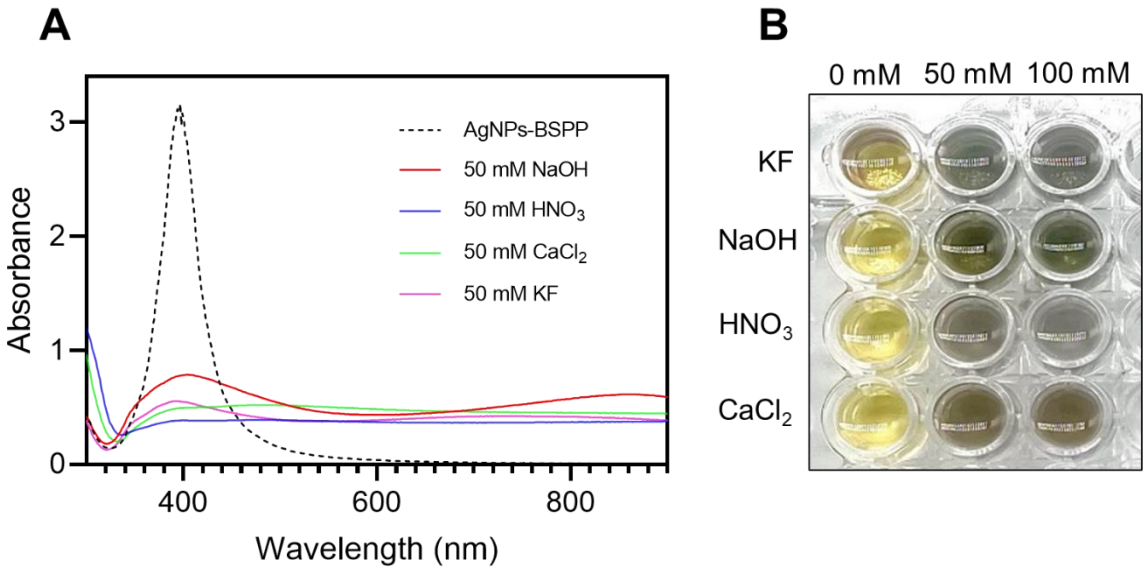

Figure S20 (A) UV-Vis spectra of AgNPs-BSPP dispersed in either 50 mM of NaOH, HNO_3, $CaCl_2$ or KF and **(B)** the corresponding pictures.

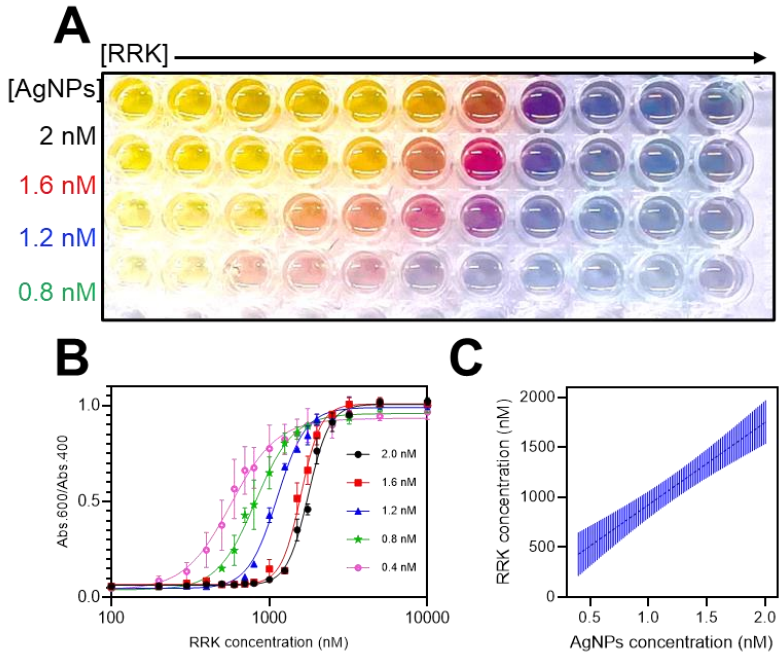

Figure S21 (A) Pictures of several samples of AgNPs-BSPP at different concentrations in particles 15 minutes after the addition of increasing concentration of RRK from 0 µM to 10 µM. **(B)** Ratio of the absorbance at 600 nm and 400 nm as a function of

RRK concentration for different concentrations in particle. **(C)** RRK concentration needed to obtain a ratio 600 nm/400 nm of 0.5 as a function of the AgNPs-BSPP concentration. Error bars are for 95% confidence interval.

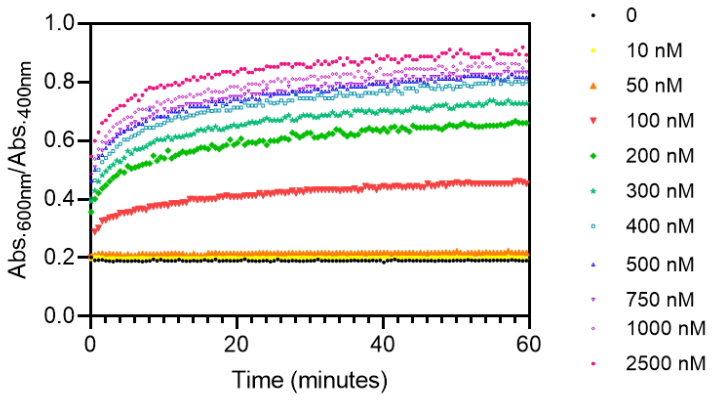

Figure S22 Evolution of the ratio of the absorbance at 600 nm and 400 nm of AgNPs-BSPP in the presence of different concentrations of RRK as a function of time.

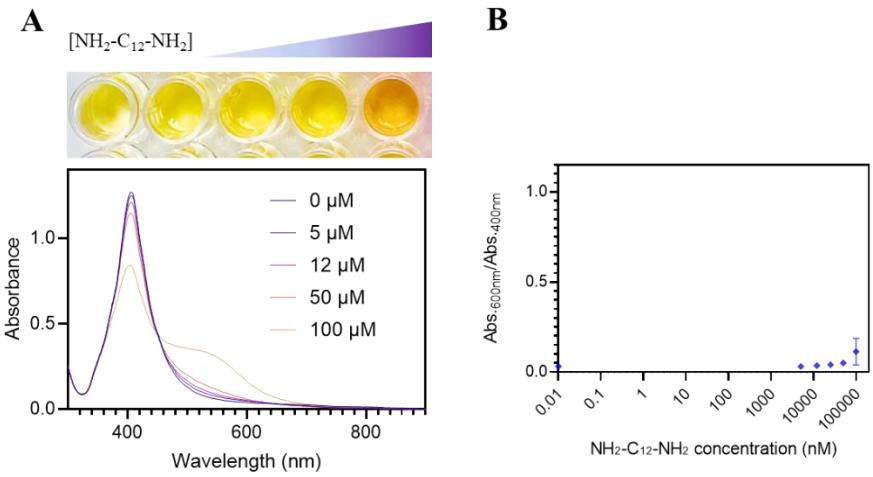

Figure S23 (A) UV-Vis spectra of several samples of 10 minutes AgNPs-BSPP in the presence of different concentrations of NH_2-C_{12}-NH_2. Inset shows the corresponding pictures. **(B)** Ratio of the absorbance at 600 nm and 400 nm as a function of the concentration of NH_2-C_{12}-NH_2. Error bars come from three experimental replicates.

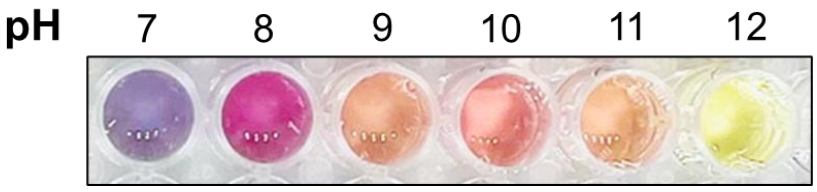

Figure S24 Pictures of the AgNPs-BSPP mixed with 1 µM of RRK as a function of pH.

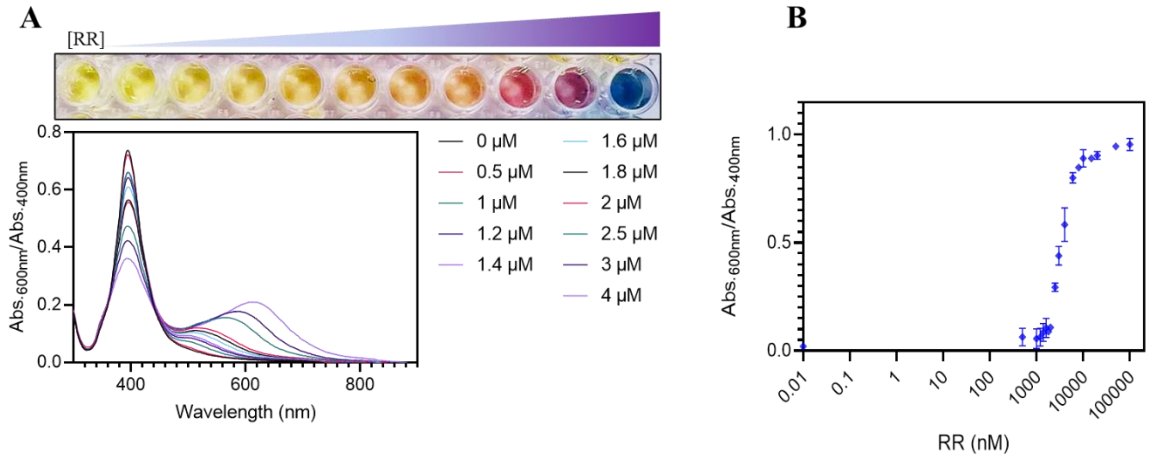

Figure S25 (A) UV-Vis spectra of several samples of AgNPs-BSPP in the presence of different concentrations of RR peptide. Inset shows the corresponding pictures. **(B)** Ratio of the absorbance at 600 nm and 400 nm as a function of the concentration of RR. Error bars come from three experimental replicates.

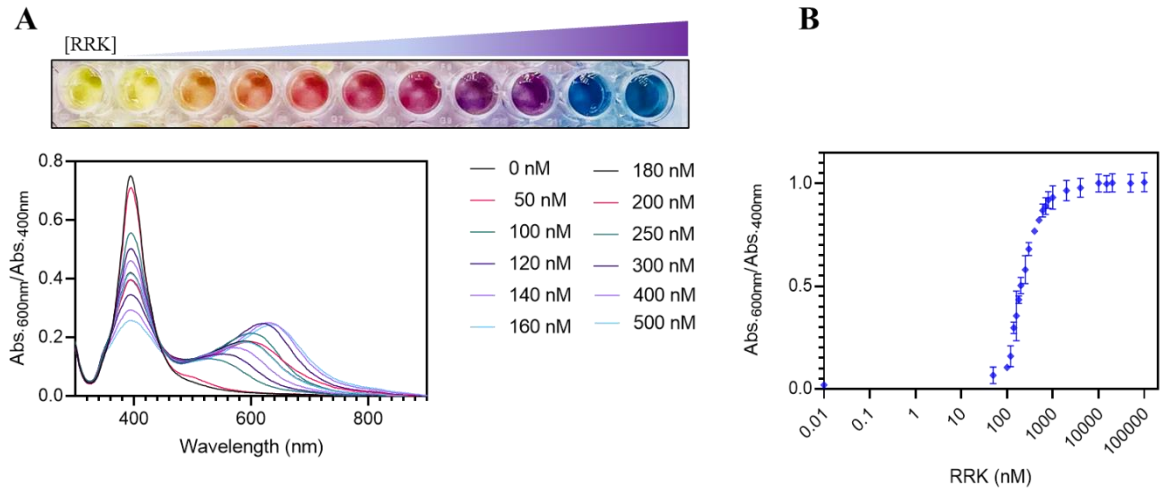

Figure S26 (A) UV-Vis spectra of several samples of AgNPs-BSPP in the presence of different concentrations of RRK. Inset shows the corresponding pictures. **(B)** Ratio of the absorbance at 600 nm and 400 nm as a function of the concentration of RRK. Error bars come from three replicates.

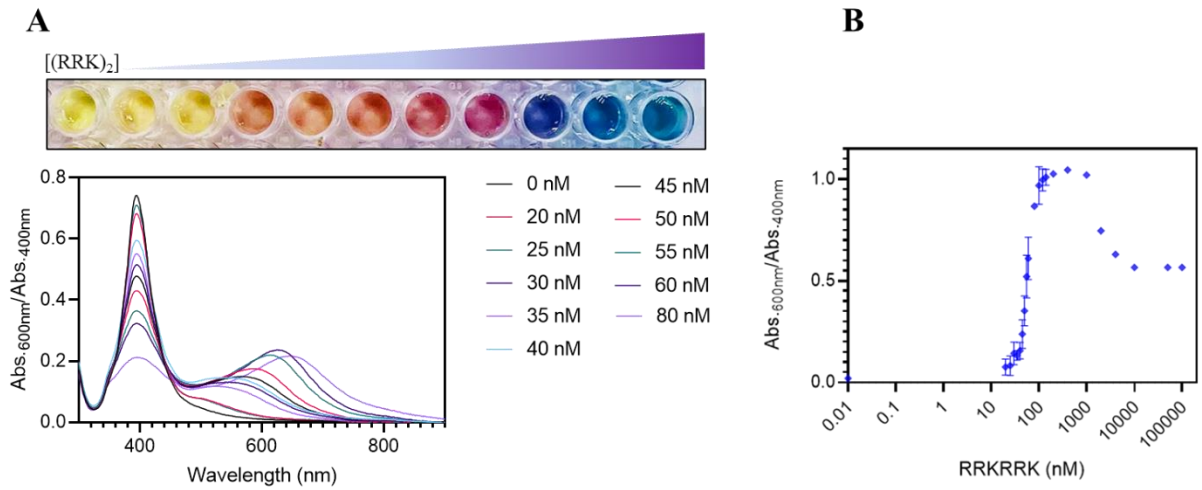

Figure S27 (A) UV-Vis spectra of several samples of AgNPs-BSPP in the presence of different concentrations of $(RRK)_2$. Inset shows the corresponding pictures. **(B)** Ratio of the absorbance at 600 nm and 400 nm as a function of the concentration of $(RRK)_2$. Error bars come from three experimental replicates.

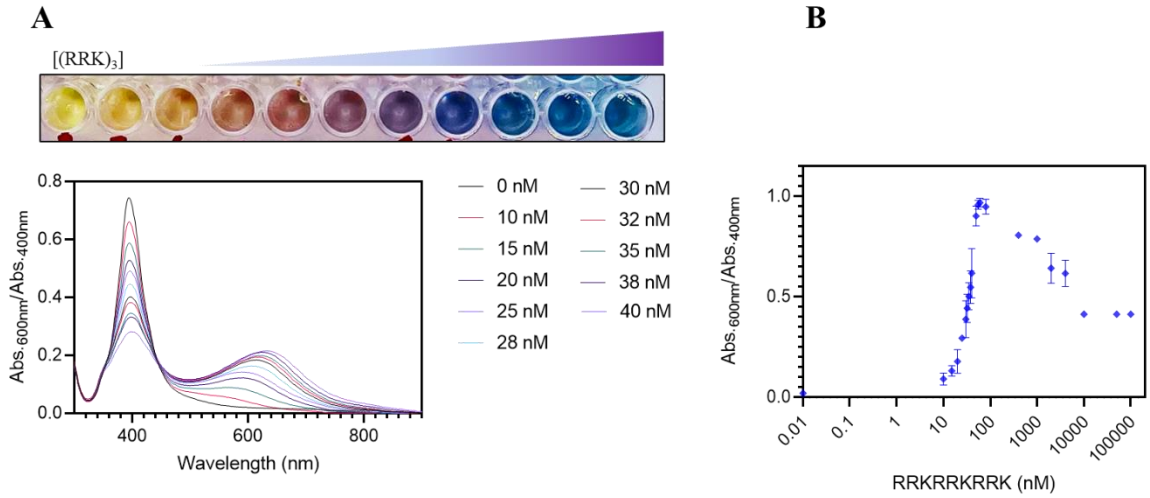

Figure S28 (A) UV-Vis spectra of several samples of AgNPs-BSPP in the presence of different concentrations of $(RRK)_3$. Inset shows the corresponding pictures. **(B)** Ratio of the absorbance at 600 nm and 400 nm as a function of the concentration of $(RRK)_3$. Error bars come from three experimental replicates.

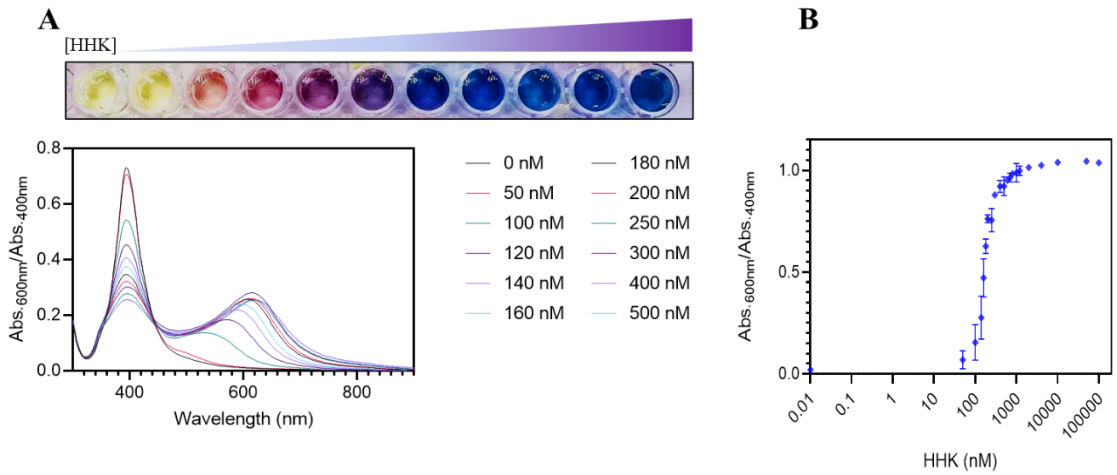

Figure S29 (A) UV-Vis spectra of several samples of AgNPs-BSPP in the presence of different concentrations of HHK. Inset shows the corresponding pictures. **(B)** Ratio of the absorbance at 600 nm and 400 nm as a function of the concentration of HHK. Error bars come from three experimental replicates.

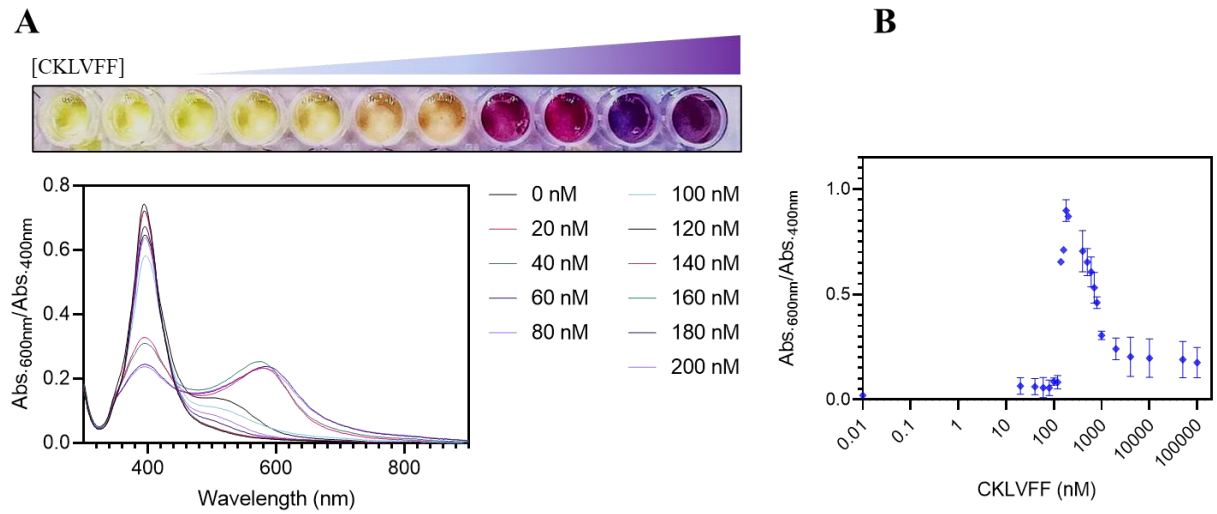

Figure S30 (A) UV-Vis spectra of several samples of AgNPs-BSPP in the presence of different concentrations of CKLVFF. Inset shows the corresponding pictures. **(B)** Ratio of the absorbance at 600 nm and 400 nm as a function of the concentration of CKLVFF. Error bars come from three experimental replicates.

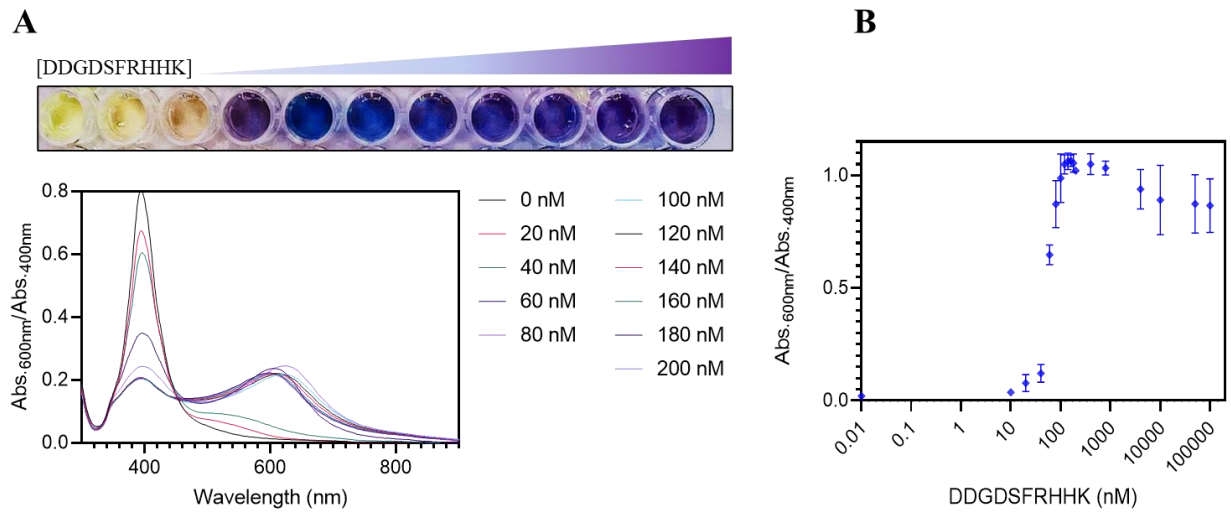

Figure S31 (A) UV-Vis spectra of several samples of AgNPs-BSPP in the presence of different concentrations of DDGDSFRHHK. Inset shows the corresponding pictures. **(B)** Ratio of the absorbance at 600 nm and 400 nm as a function of the concentration of DDGDSFRHHK. Error bars come from three experimental replicates.

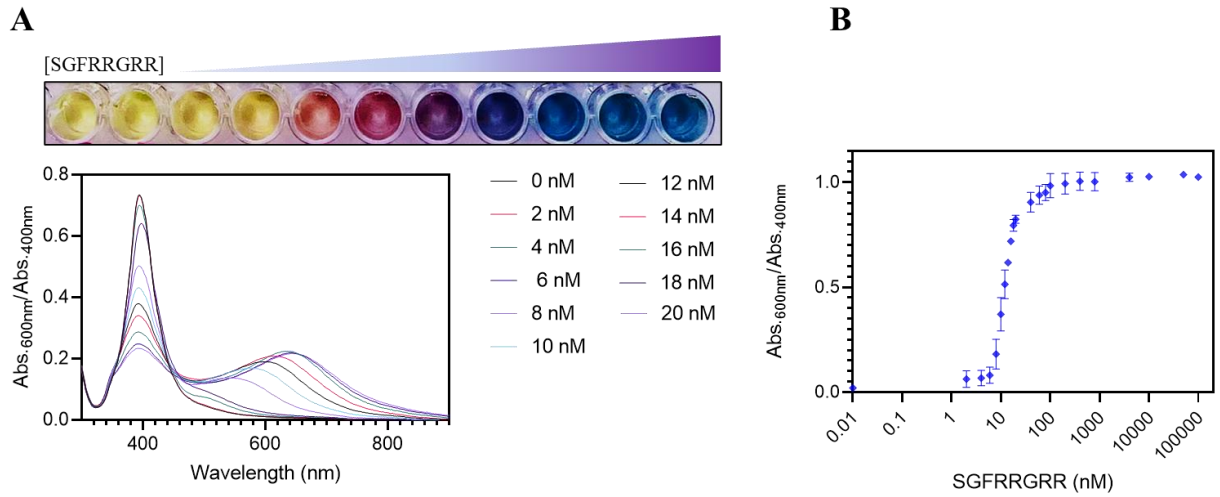

Figure S32 (A) UV-Vis spectra of several samples of AgNPs-BSPP in the presence of different concentrations of SGFRRGRR. Inset shows the corresponding pictures. **(B)** Ratio of the absorbance at 600 nm and 400 nm as a function of the concentration of SGFRRGRR. Error bars come from three experimental replicates.

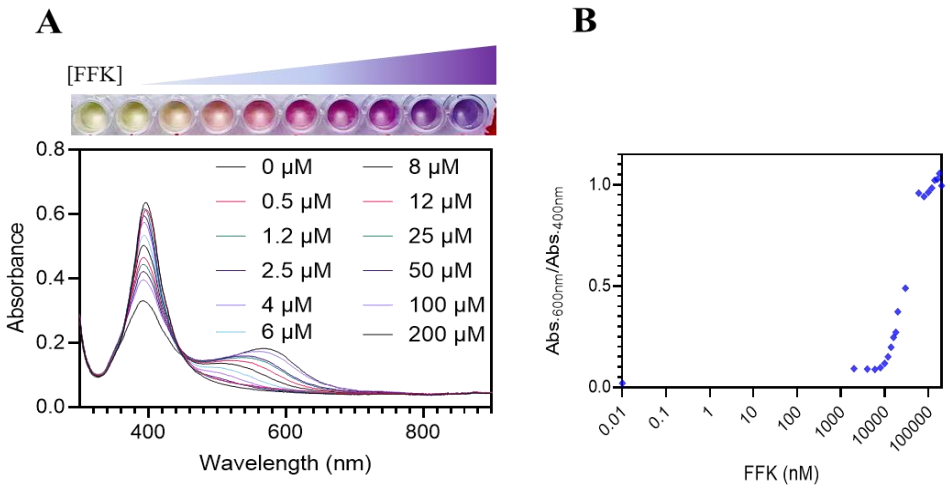

Figure S33 (A) UV-Vis spectra of several samples of AgNPs-BSPP in the presence of different concentrations of FFK. Inset shows the corresponding pictures. **(B)** Ratio of the absorbance at 600 nm and 400 nm as a function of the concentration of FFK. Error bars come from three experimental replicates.

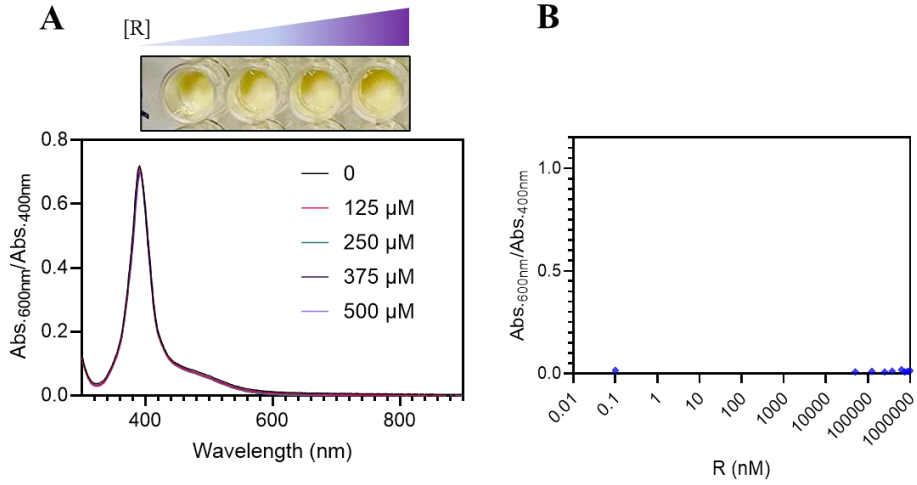

Figure S34 (A) UV-Vis spectra of several samples of AgNPs-BSPP in the presence of different concentrations of R. Inset shows the corresponding pictures. **(B)** Ratio of the absorbance at 600 nm and 400 nm as a function of the concentration of R. Error bars come from three experimental replicates.

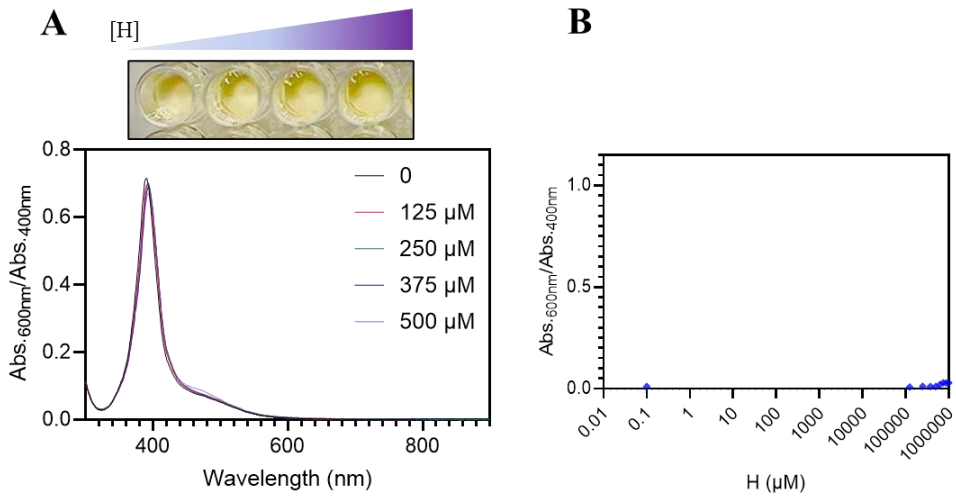

Figure S35 (A) UV-Vis spectra of several samples of AgNPs-BSPP in the presence of different concentrations of H. Inset shows the corresponding pictures. **(B)** Ratio of the absorbance at 600 nm and 400 nm as a function of the concentration of H (histadine). Error bars come from three experimental replicates.

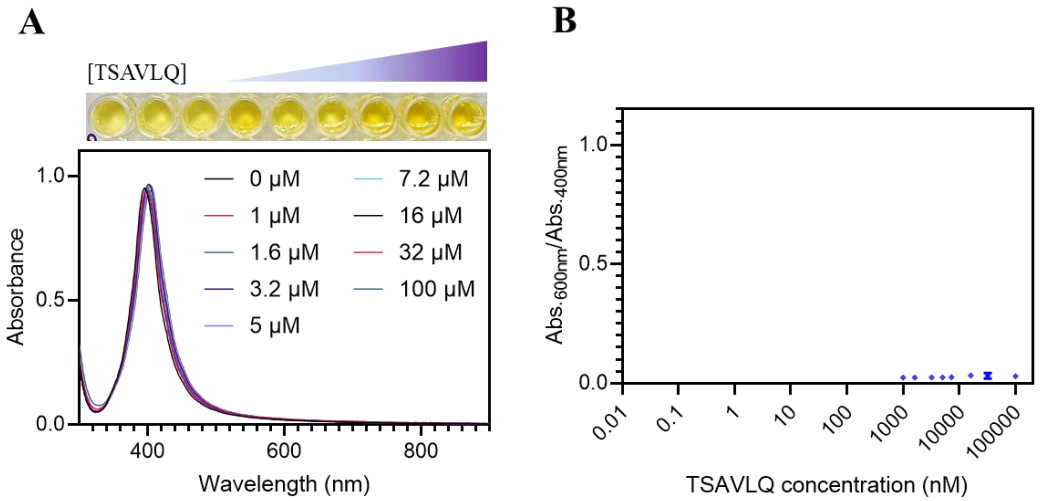

Figure S36 (A) UV-Vis spectra of several samples of AgNPs-BSPP in the presence of different concentrations of TSAVLQ. Inset shows the corresponding pictures. **(B)** Ratio of the absorbance at 600 nm and 400 nm as a function of the concentration of TSALVQ. Error bars come from three experimental replicates.

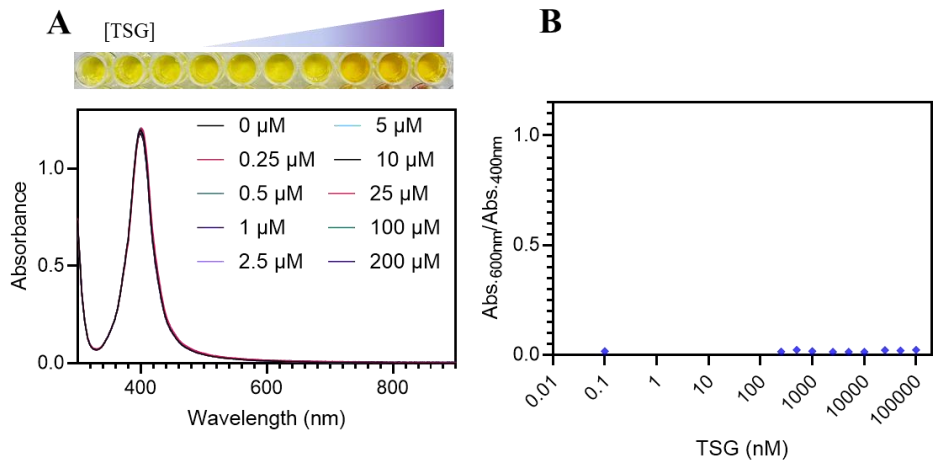

Figure S37 (A) UV-Vis spectra of several samples of AgNPs-BSPP in the presence of different concentrations of TSG. Inset shows the corresponding pictures. **(B)** Ratio of the absorbance at 600 nm and 400 nm as a function of the concentration of TSG peptide. Error bars come from three experimental replicates.

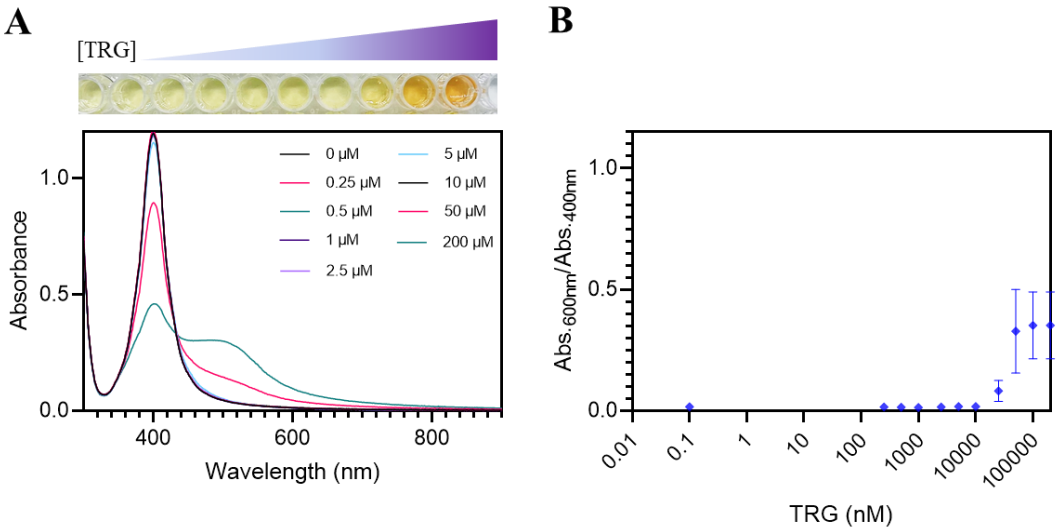

Figure S38 (A) UV-Vis spectra of several samples of AgNPs-BSPP in the presence of different concentrations of TRG peptide. Inset shows the corresponding pictures. **(B)** Ratio of the absorbance at 600 nm and 400 nm as a function of the concentration of TRG. Error bars come from three experimental replicates.

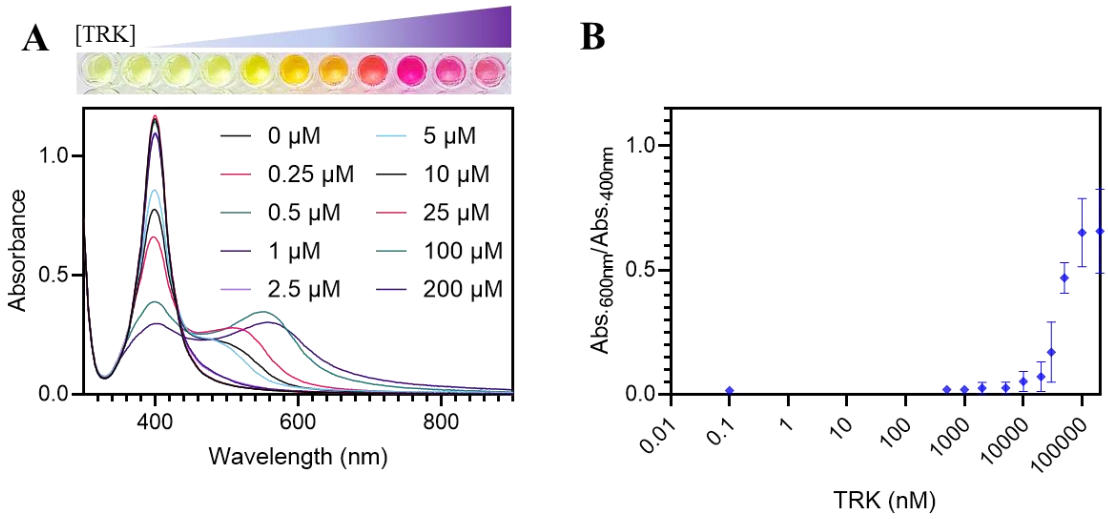

Figure S39 (A) UV-Vis spectra of several samples of AgNPs-BSPP in the presence of different concentrations of TRK peptide. Inset shows the corresponding pictures. **(B)** Ratio of the absorbance at 600 nm and 400 nm as a function of the concentration of TRK. Error bars come from three experimental replicates.

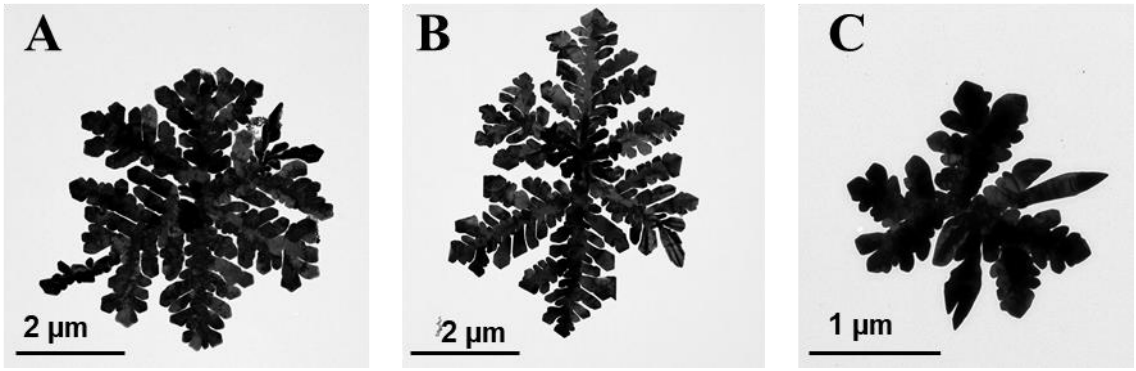

Figure S40 TEM pictures of AgNPs-BSPP that reacted either with (a) RRK, (b) HHK, or (c) FFK peptides.

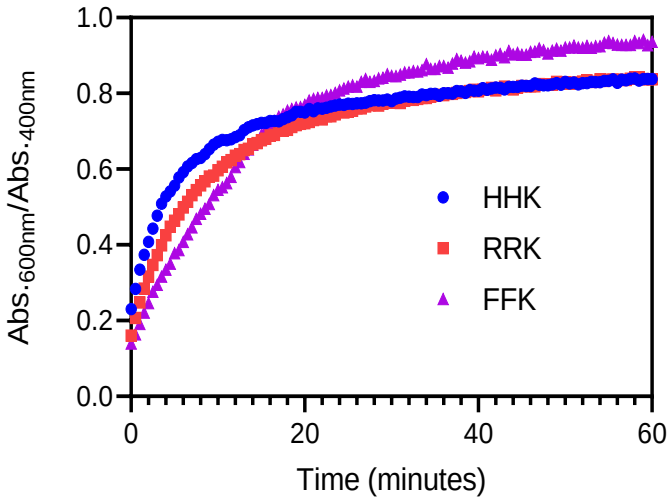

Figure S41 Evolution of the ratio of the absorbance at 600 nm and 400 nm of AgNPs-BSPP in the presence of either 1 µM of HHK, 1 µM of RRK, or 100 µM of FFK as a function of time.

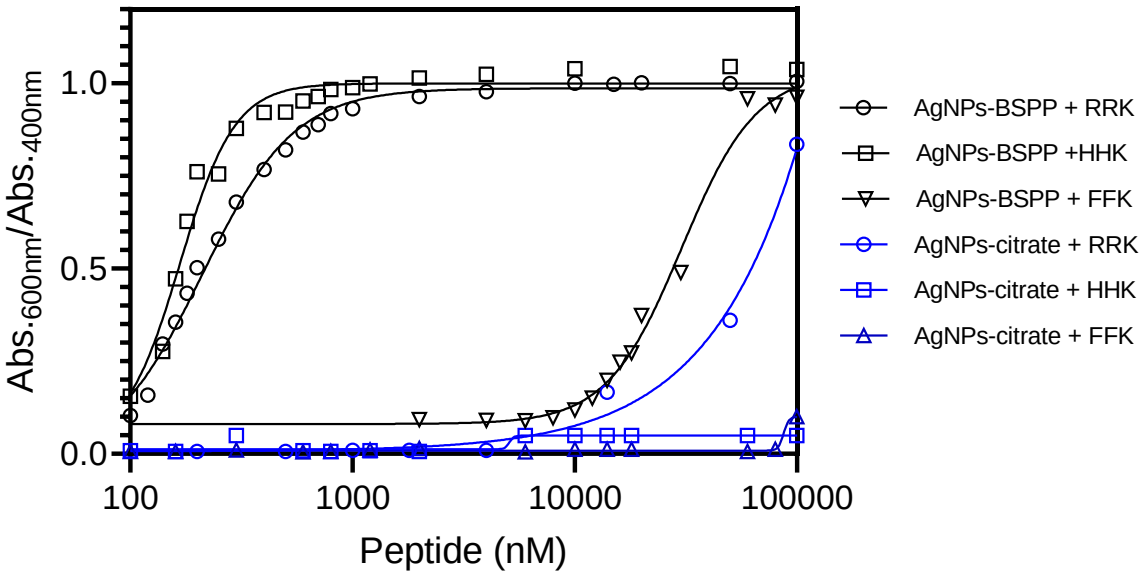

Figure S42 Ratio of the absorbance at 600 nm and 400 nm of either AgNPs-BSPP (black) or AgNPs-citrate (blue) in the presence of RRK, HHK or FFK as a function of the peptide concentration.

7. Applications

7.1 Detection of the enzymatic activity of the main protease of SARS-CoV-2 virus.

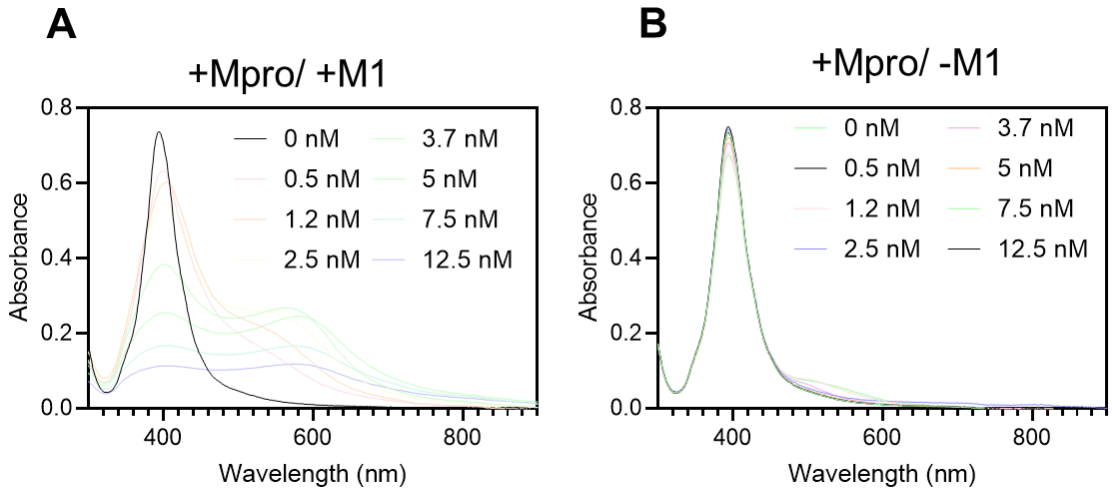

Figure S43. UV-Vis spectra of AgNPs-BSPP mixed with samples containing different concentrations of Mpro incubated **(A)** in the presence or **(B)** the absence of M1.

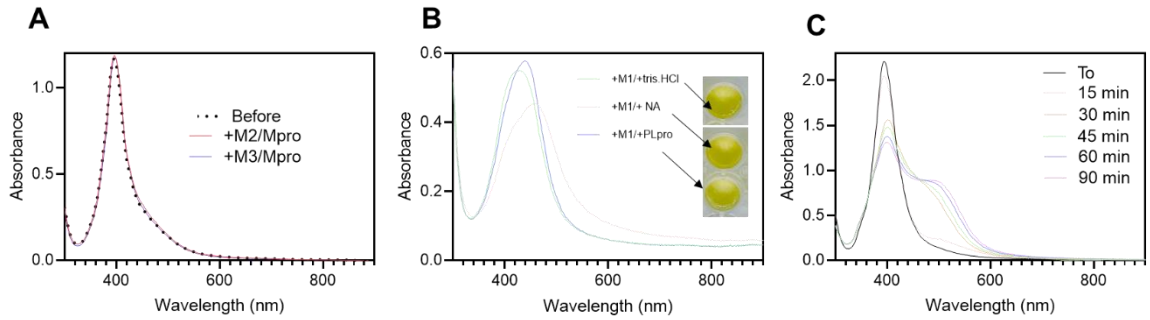

Figure S44. (A) UV-Vis spectra of different of AgNPs-BSPP mixed with sample of 12.5 nM of Mpro that was incubated with either M2 or M3. **(B)** UV-Vis spectra of AgNPs-BSPP mixed with samples of 125 nM of PLpro or NA that were incubated with M1 **(C)** UV-Vis spectra of AgNPs-BSPP mixed with M1 over time.

7.2 Sensor-array for the distinction between samples with SARS-CoV-2 or influenza proteases

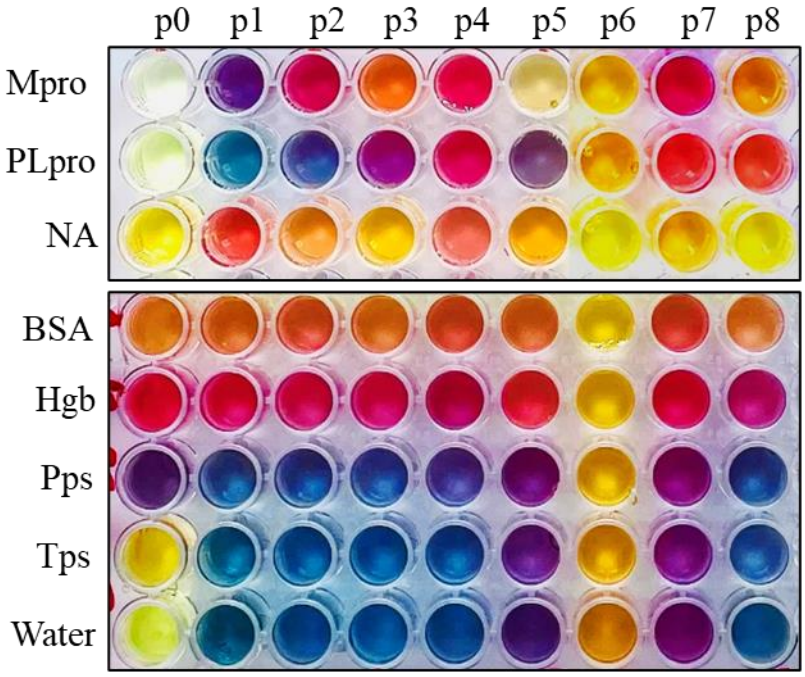

Figure S45. Picture of the sensor-array for the detection of 10 nM of Mpro, PLpro, neuraminidase (NA), BSA, hemoglobin (Hgb), pepsin (Pps), or trypsin (Tps) in water. Control = absence of target protein. P0 = absence of peptide.

Table S1. Training matrix of the optical responses (ratiometric absorbances) for the eight peptides of the sensor array used for the detection of proteins in water.

#	P1	P2	P3	P4	P5	P6	P7	p8
Water	1.044	0.989	0.950	1.054	1.065	1.009	1.072	0.832
Water	1.012	1.040	0.986	1.051	1.043	1.008	1.063	0.990
Water	1.055	1.046	1.021	1.062	1.050	1.018	1.075	1.053
Water	1.051	1.054	1.031	1.061	1.048	1.017	1.075	1.046
Hbg	0.648	0.791	0.632	0.691	0.649	0.551	0.702	0.578
Hbg	0.629	0.822	0.664	0.730	0.686	0.589	0.770	0.578
Hbg	0.497	0.589	0.773	0.662	0.686	0.613	0.524	0.718
Hbg	0.802	0.851	0.841	0.910	0.668	0.778	0.890	0.718
Tps	0.851	0.990	0.995	1.000	1.041	1.007	1.014	0.824
Tps	0.896	0.961	0.966	0.946	0.956	0.864	0.895	0.824
Tps	0.938	1.015	1.021	0.970	1.010	0.869	0.980	0.861
Tps	0.678	0.656	0.952	0.975	0.948	0.856	0.989	0.885
Pps	0.595	1.045	1.052	0.974	1.005	0.885	1.053	0.964
Pps	0.049	0.437	1.048	1.049	0.962	0.961	0.870	1.050
Pps	0.539	1.044	1.049	0.936	0.964	0.878	1.042	0.690
Pps	0.997	1.033	1.042	1.057	1.042	1.002	1.015	0.690
BSA	0.597	0.703	0.592	0.680	0.601	0.689	0.557	0.489
BSA	0.553	0.660	0.618	0.730	0.675	0.661	0.636	0.487
BSA	0.477	0.602	0.557	0.667	0.585	0.607	0.573	0.447
BSA	0.517	0.608	0.585	0.694	0.655	0.621	0.595	0.489
NA	0.674	0.641	0.672	0.779	0.680	0.711	0.685	0.684
NA	0.627	0.687	0.680	0.783	0.683	0.692	0.703	0.698
NA	0.621	0.638	0.668	0.803	0.636	0.691	0.718	0.675
NA	0.698	0.596	0.706	0.835	0.757	0.718	0.721	0.826
PLpro	1.035	0.902	0.382	1.047	0.853	0.984	1.068	0.749
PLpro	1.007	0.837	0.191	1.043	1.007	1.055	1.003	0.474
PLpro	1.009	0.841	0.213	1.048	1.024	1.040	1.005	0.464
PLpro	1.000	0.941	0.422	1.036	1.031	0.991	1.065	0.768
Mpro	1.071	0.694	0.048	1.056	0.276	1.022	1.070	0.174
Mpro	1.057	0.605	0.065	1.038	0.089	1.011	1.037	0.155
Mpro	1.075	0.797	0.069	1.031	0.147	1.009	1.085	0.298
Mpro	0.987	0.535	0.079	1.014	0.473	0.988	1.046	0.144

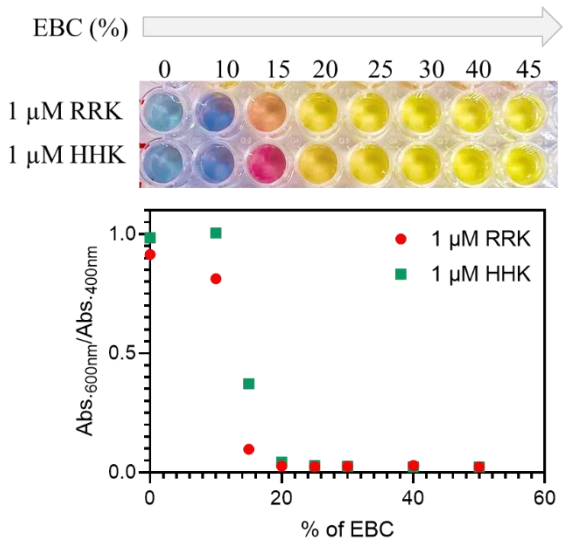

Figure S46 Ratio of the absorbance at 600 nm and 400 nm of AgNPs-BSPP mixed with 1 µM of RRK or HHK as a function of the concentration of EBC (percentage of total volume). Inset shows the corresponding pictures.

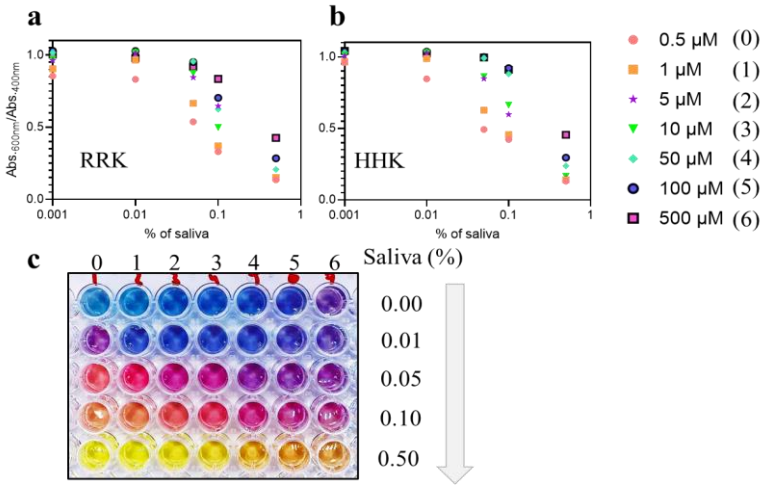

Figure S47 (a and b) Ratio of the absorbance at 600 nm and 400 nm of the AgNPs-BSPP 10 minutes after the reaction with (a) RRK or (b) HHK peptides for different concentrations of peptides as a function of the percentage of the saliva present in the sample. (c) Pictures of several samples of AgNPs-BSPP 10 minutes after the reaction with different concentrations of HHK peptides in the presence of increasing percentages of saliva.

Table S2. Summary of the peptide concentrations used for the sensor array as a function of the operating medium.

Peptide	P1	P2	P3	P4	P5	P6	P7	P8	P9
Sequence	RR	RRK	HHK	$(RRK)_2$	$(RRK)_3$	CKLVFF	DDGDSFRHHK	SGFRRGRR	FFK
Conc. (water)	10 µM	1 µM	1 µM	100 nM	60 nM	180 nM	160 nM	100 nM	100 µM
Conc. (EBC)	20 µM	4 µM	4 µM	1 µM	120 nM	3 µM	1 µM	250 nM	250 nM
Conc. (Saliva)	20 µM	4 µM	4 µM	1 µM	120 nM	3 µM	1 µM	250 nM	250 nM

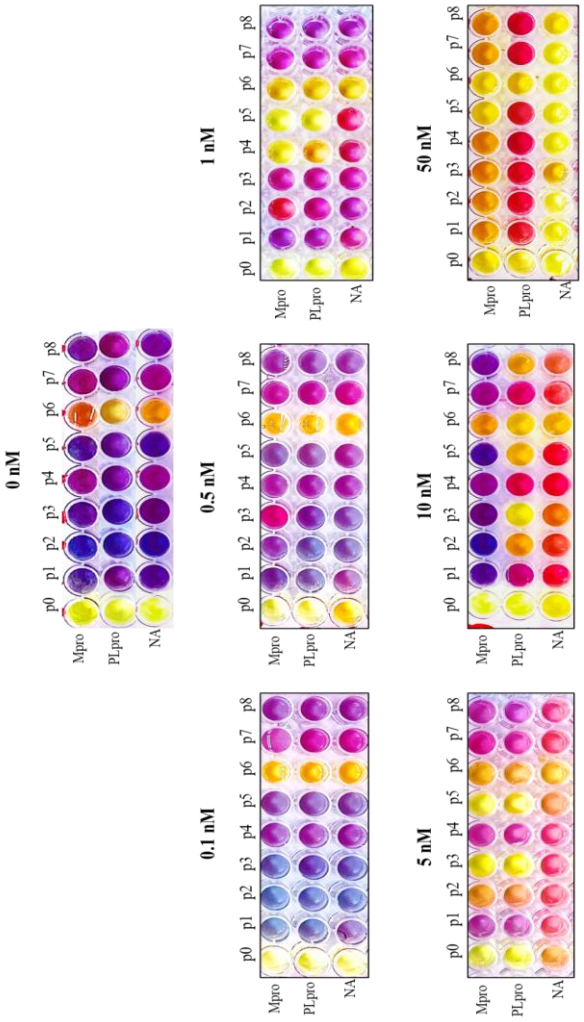

Figure S48. Pictures of the sensor array for the detection of Mpro, PLpro, and neuraminidase in EBC from 0 to 50 nM.

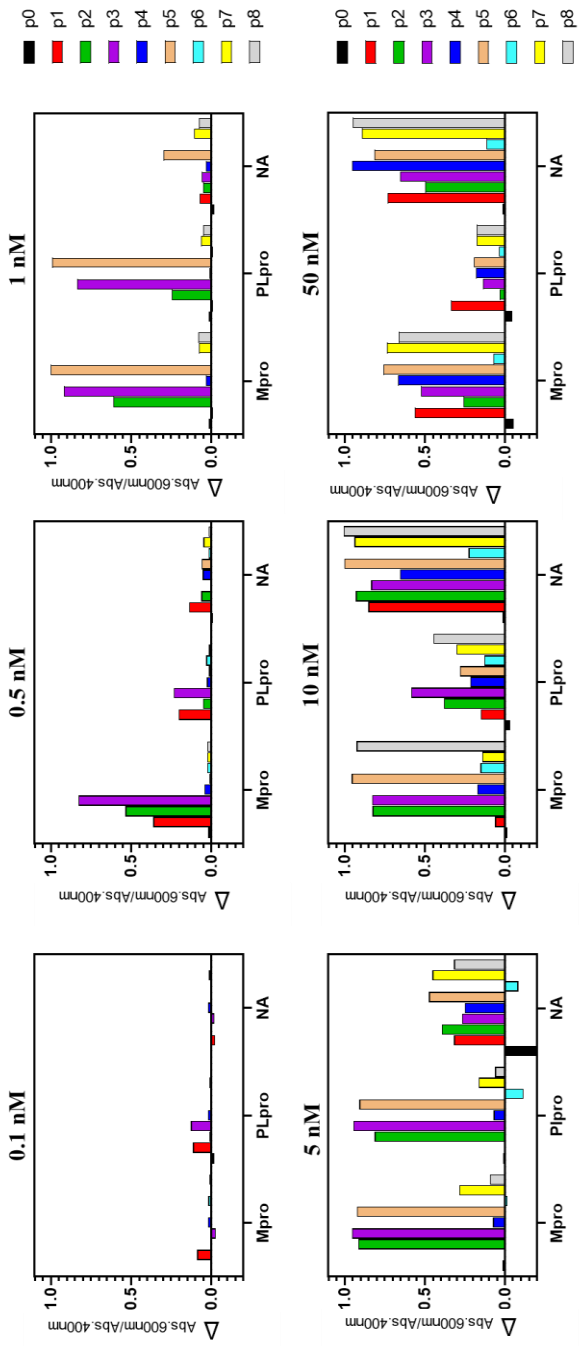

Figure S49. Optical response pattern for the detection of Mpro, PLpro, and neuraminidase at concentrations ranging from 0 nM to 50 nM in EBC obtained by subtracting the ratiometric absorbance (600 nm/400 nm) to the one at 0 nM.

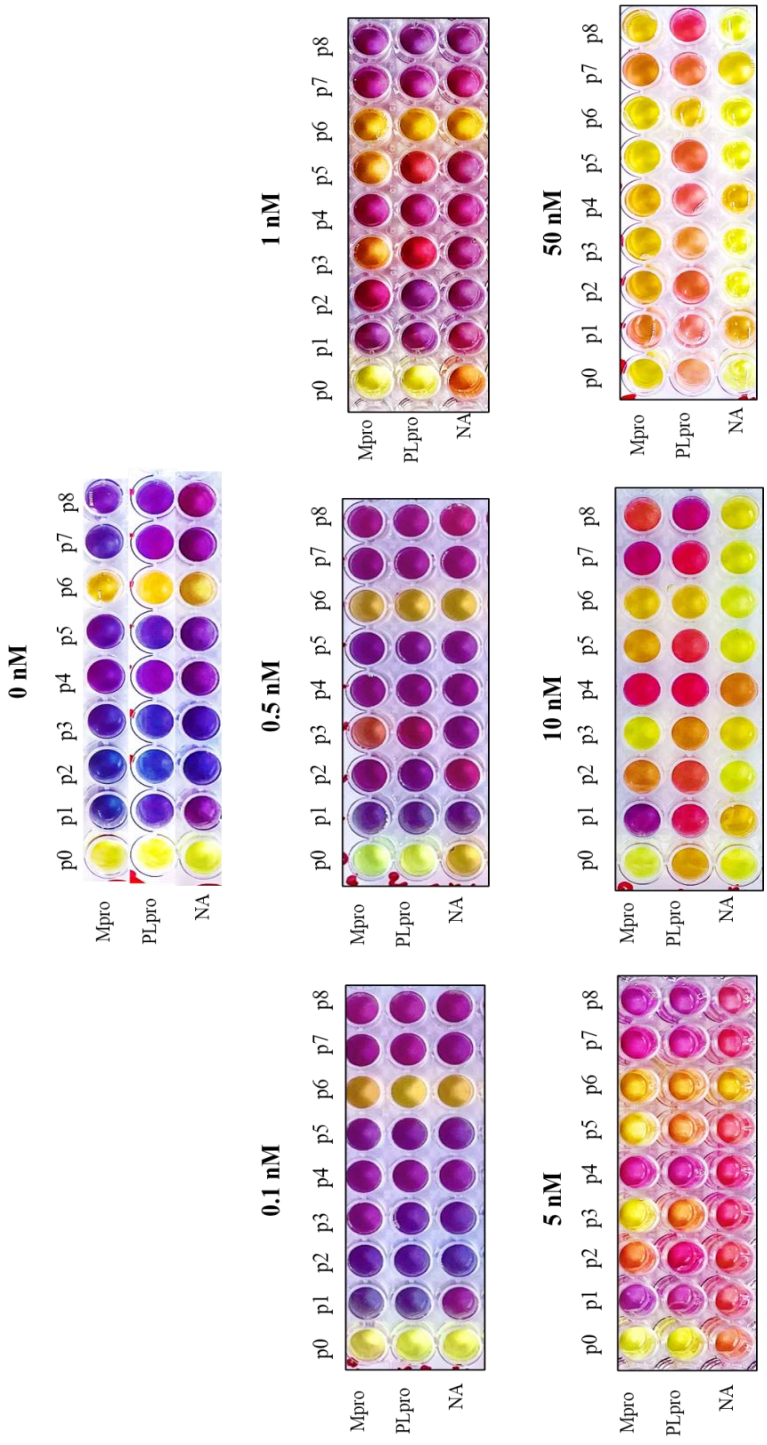

Figure S50. Pictures of the sensor array for the detection of Mpro, PLpro, and neuraminidase in saliva at concentrations ranging from 0 to 50 nM.

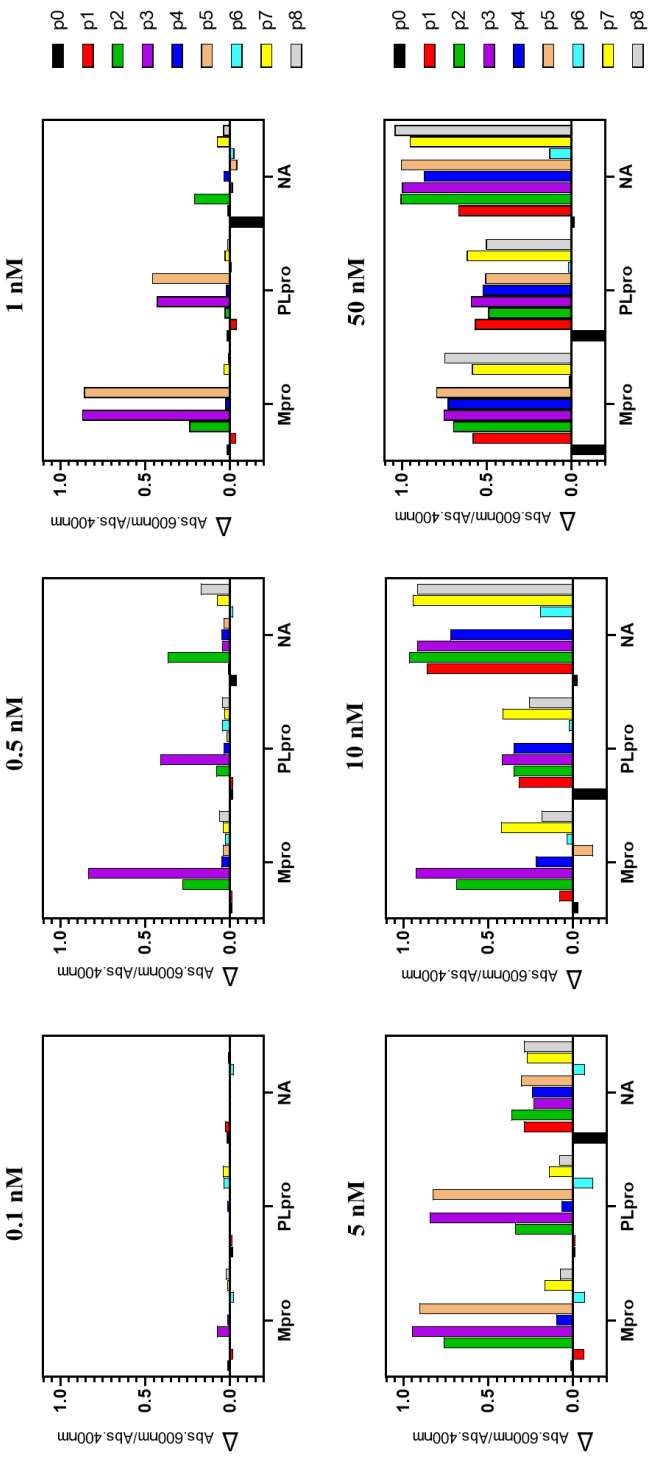

Figure S51. Optical response pattern for the detection of Mpro, PLpro and neuraminidase at concentrations ranging from 0 nM to 50 nM in saliva obtained by subtracting the ratiometric absorbance (600 nm/400 nm) to the one at 0 nM.

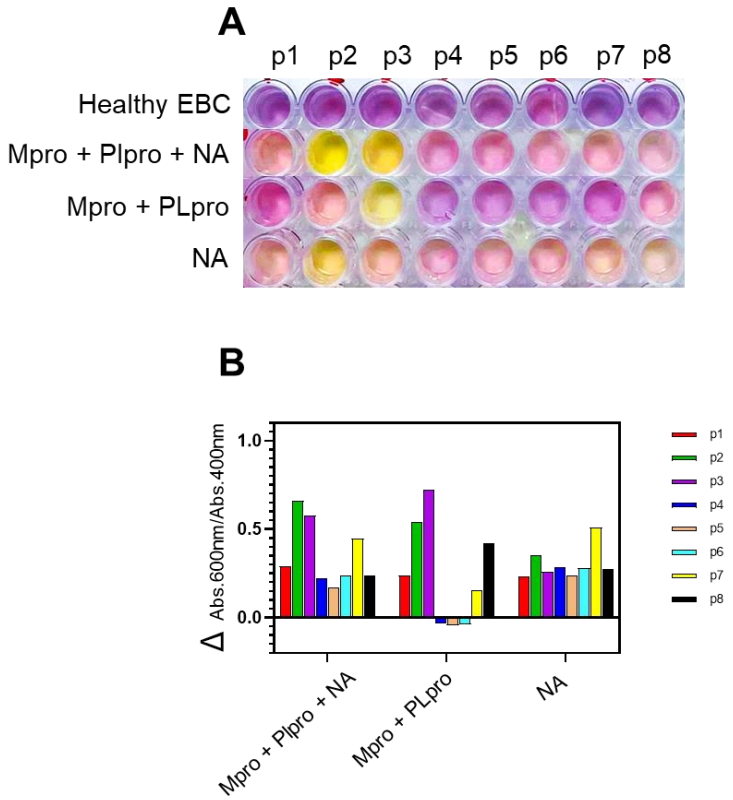

Figure S52. (A) Pictures of the sensor-array for the detection of healthy EBC spiked with a mixture of 3 nM of MPro, 3 nM of PLpro and 3 nM of NA or mixture of 3 nM of Mpro and 3 nM of PLpro or only 3 nM of NA. **(B)** The corresponding optical responses pattern obtained by subtracting the ratiometric absorbance (600 nm/400 nm) to the one of healthy EBC.

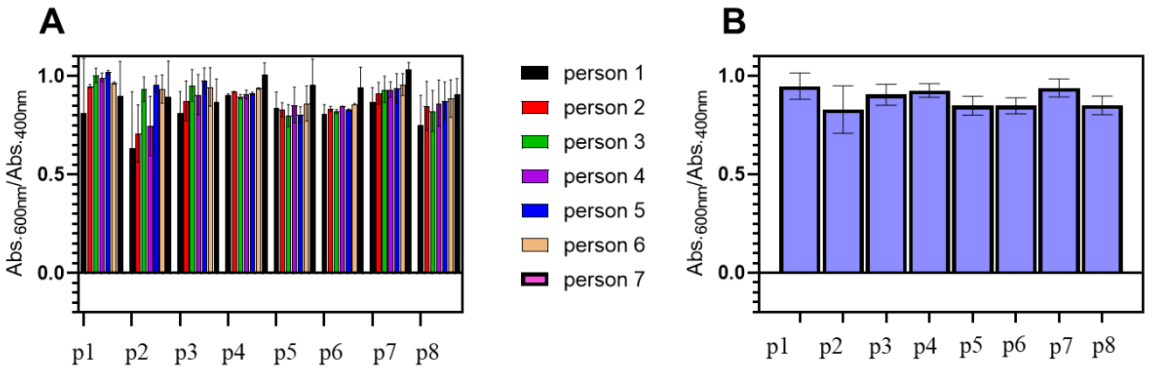

Figure S53. (A) Optical response pattern of healthy EBC coming from seven subjects PCR-negative for COVID-19. The standard deviation was obtained for three replications for each person. **(B)** Average optical response pattern for healthy EBC for each peptide obtained from seven people. The error bars represent 95% confidence intervals.

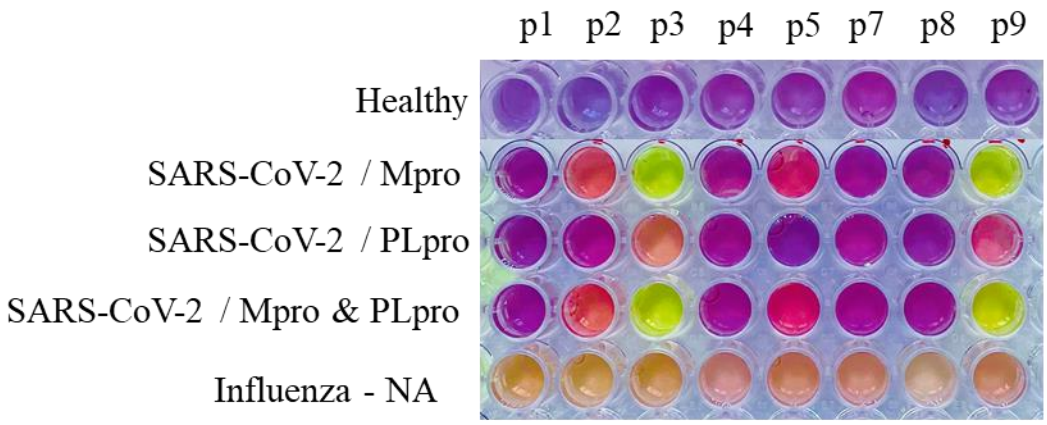

Figure S54. Pictures of the sensor-array reference: 3 nM of Mpro, PLpro, Mpro and PLpro, or NA spiked in negative EBC.

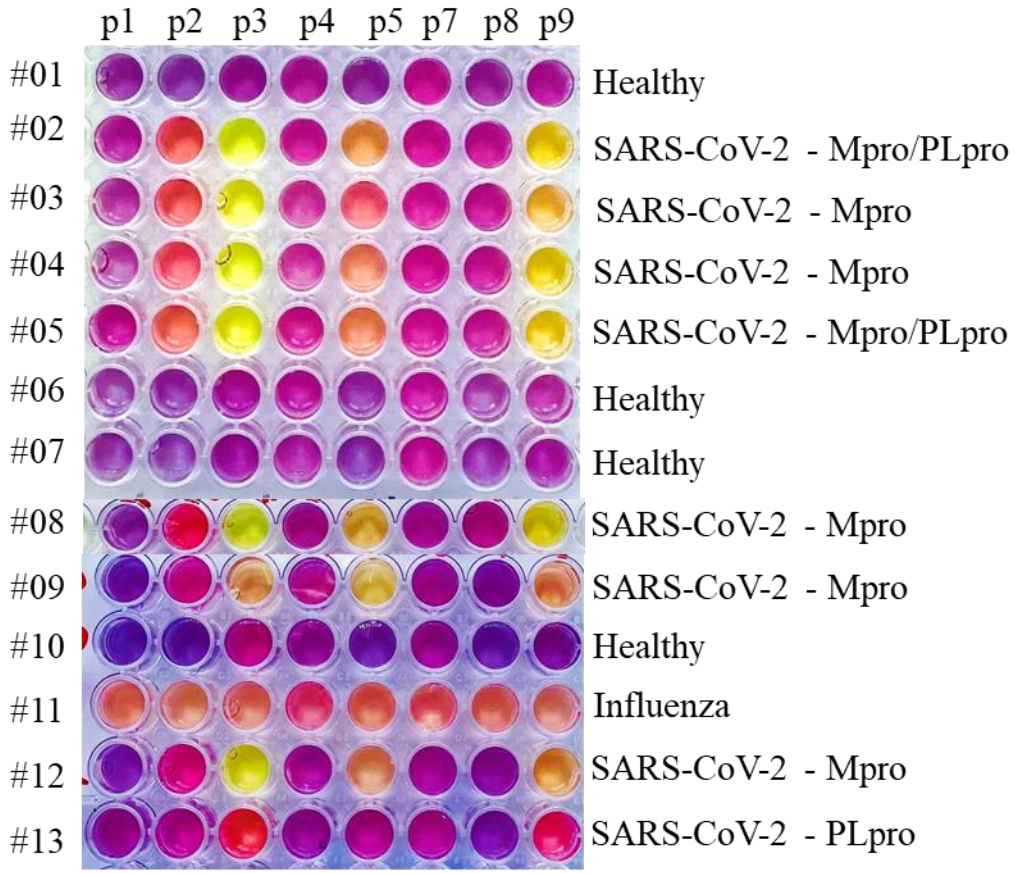

Figure S55. Pictures of the sensor-array for the samples #01 to #13.

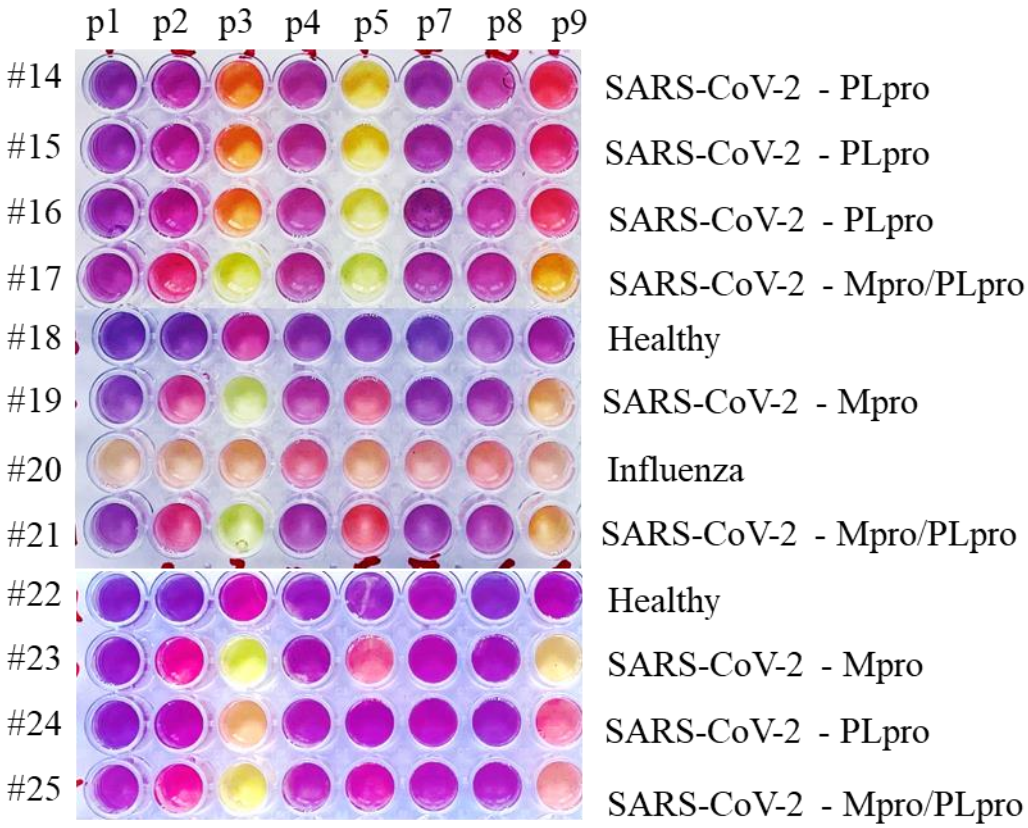

Figure S56. Pictures of the sensor-array for the samples #14 to #25.

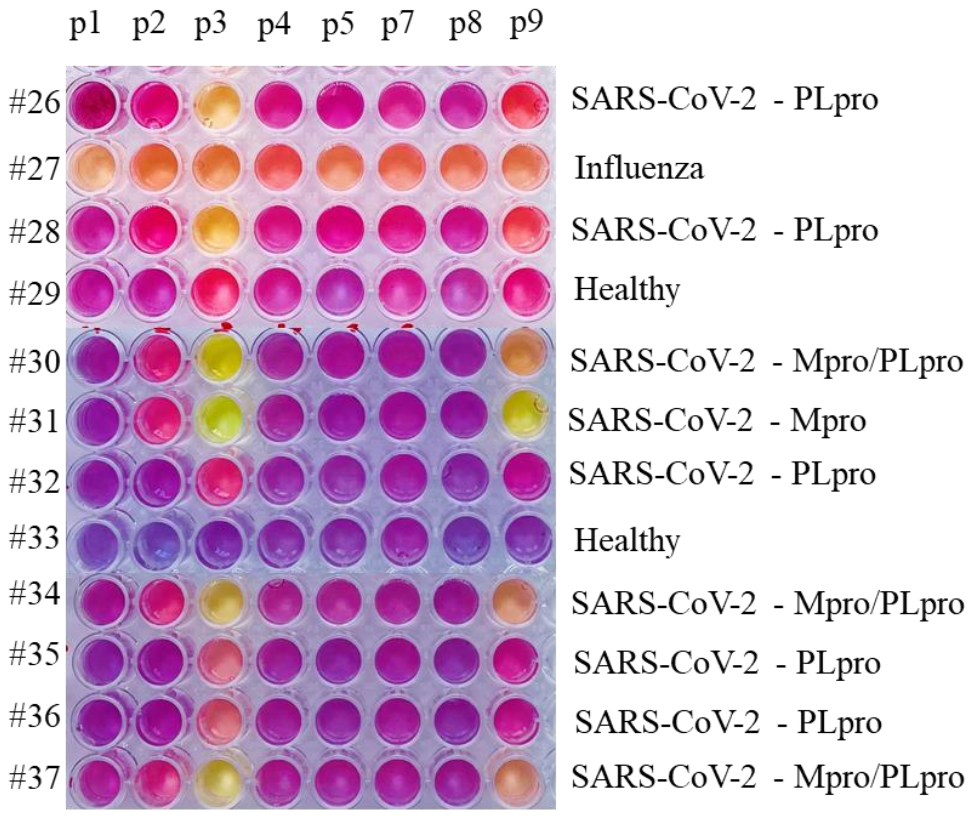

Figure S57. Pictures of the sensor-array for the samples #26 to #37.

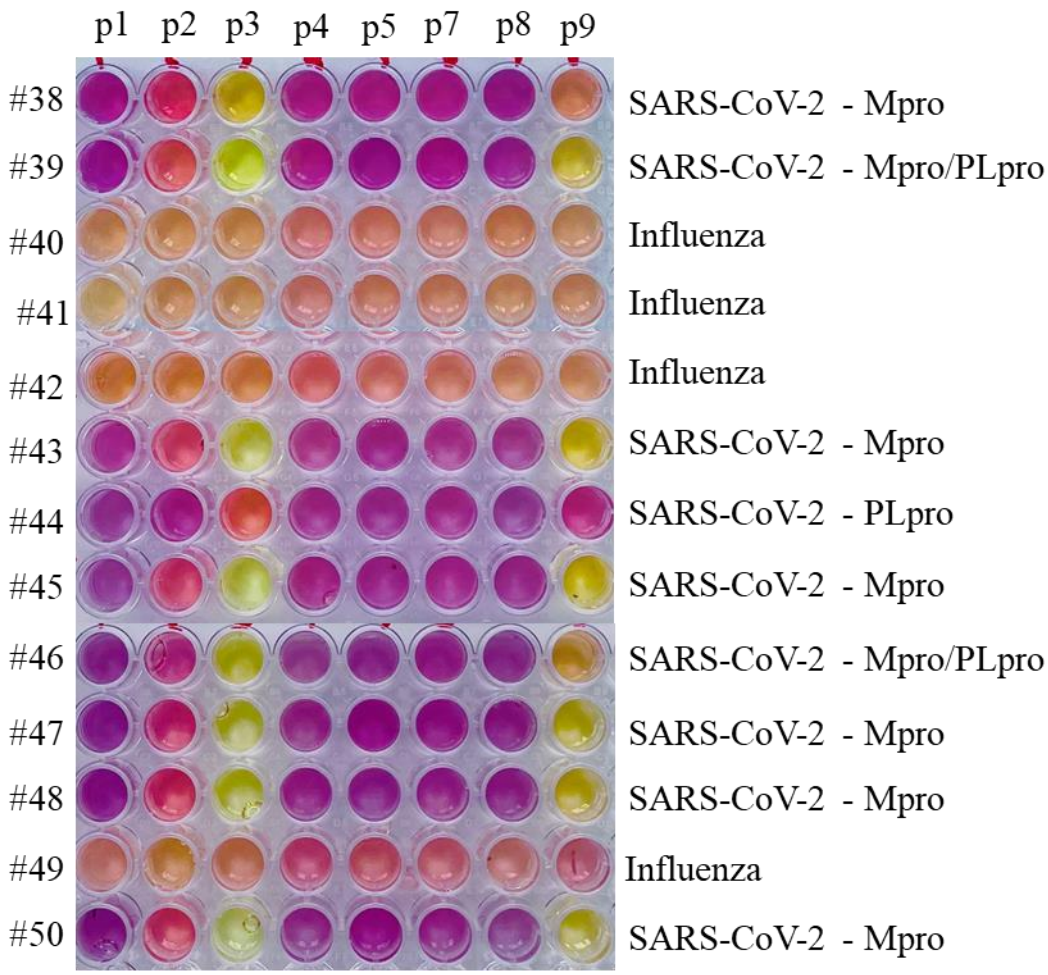

Figure S58. Pictures of the sensor-array for the samples #38 to #50.

Table S4. Results of the blind study containing the ratiometric absorbance pattern for each peptide, the diagnosis identified by the naked eyes, and the composition of the sample. Healthy = nothing added

	Ratiometric absorbance response pattern								Identification	Verification
#	P1	P2	P3	P4	P5	P7	P8	p9	Virus	Protein
1	1.012	1.040	0.986	1.051	1.043	1.008	1.063	0.990	Healthy	Healthy
2	1.018	0.531	0.057	1.045	0.162	1.016	1.054	0.168	SARS-CoV-2	Mpro&PLpro
3	1.076	0.582	0.068	1.056	0.441	1.019	1.065	0.275	SARS-CoV-2	Mpro
4	1.071	0.694	0.048	1.056	0.276	1.022	1.070	0.174	SARS-CoV-2	Mpro
5	1.045	0.711	0.076	1.051	0.288	1.012	1.060	0.280	SARS-CoV-2	Mpro&PLpro
6	1.055	1.046	1.021	1.062	1.050	1.018	1.075	1.053	Healthy	Healthy
7	1.051	1.054	1.031	1.061	1.048	1.017	1.075	1.046	Healthy	Healthy
8	1.057	0.605	0.065	1.038	0.089	1.011	1.037	0.155	SARS-CoV-2	Mpro
9	1.008	0.569	0.201	1.033	0.084	1.003	1.028	0.229	SARS-CoV-2	Mpro
10	1.032	1.040	0.735	1.052	1.051	1.013	1.067	1.003	Healthy	Healthy
11	0.674	0.641	0.672	0.779	0.680	0.711	0.685	0.684	Influenza	NA
12	1.075	0.797	0.069	1.031	0.147	1.009	1.085	0.298	SARS-CoV-2	Mpro
13	1.035	0.902	0.382	1.047	0.853	0.984	1.068	0.749	SARS-CoV-2	PLpro
14	0.987	0.822	0.181	1.039	0.980	1.056	0.994	0.355	SARS-CoV-2	PLpro
15	1.007	0.837	0.191	1.043	1.007	1.055	1.003	0.474	SARS-CoV-2	PLpro
16	1.009	0.841	0.213	1.048	1.024	1.040	1.005	0.464	SARS-CoV-2	PLpro
17	1.013	0.724	0.111	1.040	1.011	1.057	1.005	0.317	SARS-CoV-2	Mix
18	0.988	0.949	0.984	1.053	1.050	1.067	1.010	0.839	Healthy	Healthy
19	1.034	0.729	0.078	0.964	0.513	1.057	0.994	0.320	SARS-CoV-2	Mpro&PLpro
20	0.621	0.638	0.668	0.803	0.636	0.691	0.718	0.675	Influenza	NA
21	1.042	0.820	0.096	1.047	0.552	1.066	1.006	0.445	SARS-CoV-2	Mpro&PLpro
22	0.961	0.958	0.808	1.035	1.037	0.993	1.047	0.831	Healthy	Healthy
23	0.987	0.535	0.079	1.014	0.473	0.988	1.046	0.144	SARS-CoV-2	Mpro
24	0.996	0.797	0.171	1.030	0.988	0.998	1.050	0.440	SARS-CoV-2	PLpro
25	0.997	0.658	0.130	1.003	0.937	0.954	1.018	0.435	SARS-CoV-2	Mpro&PLpro
26	0.897	0.702	0.095	1.034	0.883	0.991	1.053	0.415	SARS-CoV-2	Plpro
27	0.627	0.687	0.680	0.783	0.683	0.692	0.703	0.698	Influenza	NA
28	1.021	0.786	0.118	1.039	0.893	1.000	1.065	0.490	SARS-CoV-2	PLpro
29	1.044	0.989	0.950	1.054	1.065	1.009	1.072	0.832	Healthy	Healthy
30	0.915	0.460	0.080	0.984	0.948	0.961	1.024	0.193	SARS-CoV-2	Mpro&Plpro
31	0.983	0.527	0.059	1.014	1.031	0.992	1.055	0.090	SARS-CoV-2	Mpro
32	1.000	0.941	0.422	1.036	1.031	0.991	1.065	0.768	SARS-CoV-2	PLpro
33	1.037	1.045	0.992	1.054	1.055	1.006	1.069	1.038	Healthy	Healthy
34	0.894	0.506	0.103	0.952	0.949	0.916	1.017	0.257	SARS-CoV-2	Mpro&Plpro
35	1.023	0.910	0.317	1.046	1.050	0.997	1.061	0.630	SARS-CoV-2	PLpro
36	1.000	0.914	0.351	1.032	1.045	0.994	1.067	0.728	SARS-CoV-2	PLpro
37	0.979	0.713	0.121	1.006	1.016	0.958	1.037	0.358	SARS-CoV-2	Mpro&PLpro
38	0.918	0.522	0.115	0.977	0.953	0.929	1.011	0.332	SARS-CoV-2	Mpro&PLpro
39	1.003	0.520	0.063	1.017	1.030	0.983	1.036	0.151	SARS-CoV-2	Mpro
40	0.633	0.647	0.650	0.757	0.696	0.687	0.686	0.651	Influenza	NA
41	0.609	0.663	0.664	0.750	0.706	0.691	0.662	0.669	Influenza	NA
42	0.626	0.642	0.642	0.744	0.679	0.672	0.639	0.643	Influenza	NA
43	0.985	0.668	0.072	1.024	1.042	0.983	1.061	0.175	SARS-CoV-2	Mpro
44	1.037	0.937	0.385	1.042	1.047	1.000	1.065	0.857	SARS-CoV-2	PLpro
45	1.056	0.758	0.078	1.036	1.050	1.009	1.066	0.226	SARS-CoV-2	Mpro
46	0.952	0.507	0.059	1.028	0.992	0.977	1.042	0.153	SARS-CoV-2	Mpro&PLpro
47	0.993	0.507	0.060	1.047	0.770	1.005	1.061	0.096	SARS-CoV-2	Mpro
48	0.988	0.491	0.056	1.049	1.050	0.997	1.074	0.140	SARS-CoV-2	Mpro
49	0.698	0.596	0.706	0.835	0.757	0.718	0.721	0.826	Influenza	NA
50	1.020	0.594	0.154	1.062	0.810	1.014	1.069	0.168	SARS-CoV-2	Mpro

Table S5. Training matrix of the optical responses (ratiometric absorbances) for the eight peptides of the sensor array used for the detection of Mpro, PLpro, Mpro and PLpro, or NA spiked in healthy EBC. Healthy = nothing added.

#	P1	P2	P3	P4	P5	P7	P8	p9
Healthy	1.044	0.989	0.950	1.054	1.065	1.009	1.072	0.832
Healthy	1.012	1.040	0.986	1.051	1.043	1.008	1.063	0.990
Healthy	1.055	1.046	1.021	1.062	1.050	1.018	1.075	1.053
Healthy	1.051	1.054	1.031	1.061	1.048	1.017	1.075	1.046
Healthy	1.032	1.040	0.735	1.052	1.051	1.013	1.067	1.003
Healthy	0.988	0.949	0.984	1.053	1.050	1.067	1.010	0.839
Healthy	0.961	0.958	0.808	1.035	1.037	0.993	1.047	0.831
Mpro&Plpro	1.018	0.531	0.057	1.045	0.162	1.016	1.054	0.168
Mpro&PLpro	1.042	0.820	0.096	1.047	0.552	1.066	1.006	0.445
Mpro&Plpro	1.045	0.711	0.076	1.051	0.288	1.012	1.060	0.280
Mpro&PLpro	1.013	0.724	0.111	1.040	1.011	1.057	1.005	0.317
Mpro&PLpro	0.979	0.713	0.121	1.006	1.016	0.958	1.037	0.358
Mpro&PLpro	0.918	0.522	0.115	0.977	0.953	0.929	1.011	0.332
Mpro&PLpro	0.952	0.507	0.059	1.028	0.992	0.977	1.042	0.153
NA	0.674	0.641	0.672	0.779	0.680	0.711	0.685	0.684
NA	0.627	0.687	0.680	0.783	0.683	0.692	0.703	0.698
NA	0.621	0.638	0.668	0.803	0.636	0.691	0.718	0.675
NA	0.698	0.596	0.706	0.835	0.757	0.718	0.721	0.826
NA	0.633	0.647	0.650	0.757	0.696	0.687	0.686	0.651
NA	0.609	0.663	0.664	0.750	0.706	0.691	0.662	0.669
NA	0.626	0.642	0.642	0.744	0.679	0.672	0.639	0.643
PLpro	1.035	0.902	0.382	1.047	0.853	0.984	1.068	0.749
PLpro	1.007	0.837	0.191	1.043	1.007	1.055	1.003	0.474
PLpro	1.009	0.841	0.213	1.048	1.024	1.040	1.005	0.464
PLpro	1.000	0.941	0.422	1.036	1.031	0.991	1.065	0.768
PLpro	1.023	0.910	0.317	1.046	1.050	0.997	1.061	0.630
PLpro	1.000	0.914	0.351	1.032	1.045	0.994	1.067	0.728
PLpro	1.037	0.937	0.385	1.042	1.047	1.000	1.065	0.857
Mpro	1.071	0.694	0.048	1.056	0.276	1.022	1.070	0.174
Mpro	1.057	0.605	0.065	1.038	0.089	1.011	1.037	0.155
Mpro	1.075	0.797	0.069	1.031	0.147	1.009	1.085	0.298
Mpro	0.987	0.535	0.079	1.014	0.473	0.988	1.046	0.144
Mpro	1.003	0.520	0.063	1.017	1.030	0.983	1.036	0.151
Mpro	0.993	0.507	0.060	1.047	0.770	1.005	1.061	0.096
Mpro	0.988	0.491	0.056	1.049	1.050	0.997	1.074	0.140

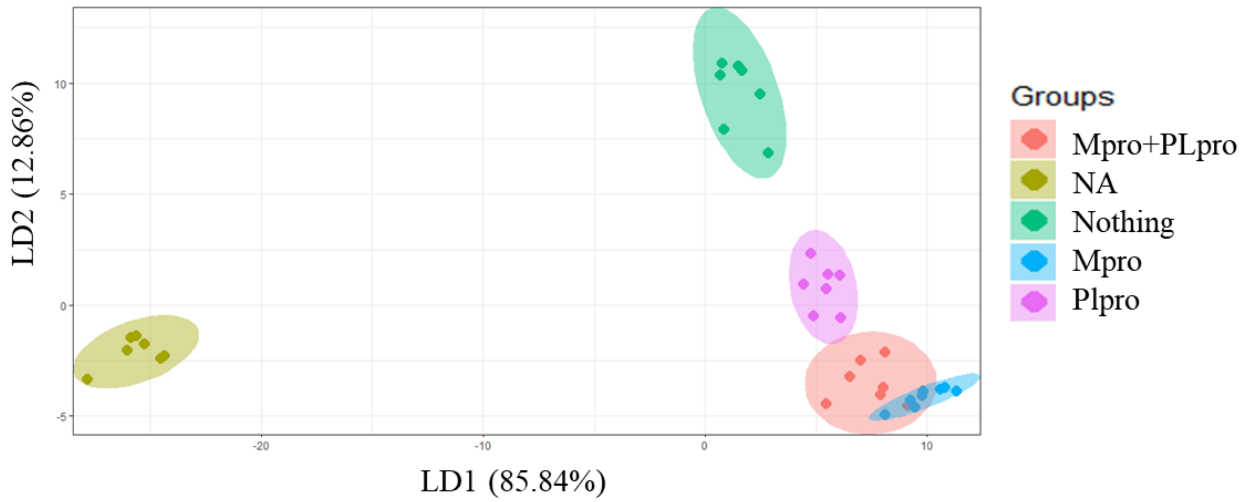

Figure S59. Canonical score plot for the first two factors of simplified ratiometric absorbance response patterns obtained with sensor-array against proteins with 3 nM concentration spiked in EBC. The canonical scores were calculated by LDA for the identification of four proteins with 95% confidence ellipses for the individual proteins shown. Data come from Table S5.

Table S6. Test matrix of the optical responses (ratiometric absorbances) for the eight peptides obtained with three healthy samples of EBC spiked with either Mpro and PLpro, NA, or nothing (Healthy).

#	P1	P2	P3	P4	P5	P7	P8	p9
Healthy	0.996	1.063	1.028	1.028	1.053	0.960	1.037	0.975
Healthy	1.022	1.037	0.973	1.049	1.051	1.011	1.068	1.023
Healthy	1.037	1.045	0.992	1.054	1.055	1.006	1.069	1.038
Mpro&PLpro	1.034	0.729	0.078	0.964	0.513	1.057	0.994	0.320
Mpro&PLpro	0.997	0.658	0.130	1.003	0.937	0.954	1.018	0.435
Mpro&PLpro	0.894	0.506	0.103	0.952	0.949	0.916	1.017	0.257
NA	0.615	0.568	0.630	0.719	0.681	0.645	0.526	0.722
NA	0.528	0.686	0.641	0.737	0.775	0.633	0.759	0.755
NA	0.656	0.611	0.702	0.766	0.880	0.580	0.727	0.621